공학석사학위논문

공압 가변 강성 액추에이터를 이용한 충격을 흡수하는 발 지지 장치

A Shock-Absorbing Foot Orthotic Device using Pneumatic Variable Stiffness Actuators

2021 년 8 월

서울대학교 대학원

기계공학부

박 영 준

공압 가변 강성 액추에이터를 이용한 충격을 흡수하는 발 지지 장치

A Shock-Absorbing Foot Orthotic Device using Pneumatic Variable Stiffness Actuators

지도교수 조 규 진

이 논문을 공학석사 학위논문으로 제출함

2021 년 4 월

서울대학교 대학원
기계공학부
박 영 준

박 영 준의 공학석사 학위논문을 인준함

2021 년 6 월

위 원 장 : 이 경 수

부위원장 : 조 규 진

위 원 : 이 동 준

Abstract

A Shock-Absorbing Foot Orthotic Device using Pneumatic Variable Stiffness Actuators

YoungJune Park
Department of Mechanical Engineering
The Graduate School
Seoul National University

The terrestrial locomotion is an indispensable element of the activities of daily living (ADL). This is established by a series of following phases: thrust, flight, and landing. During the locomotion, the ground reaction force (GRF) has a duality which enhances human motor performance as a thrust force, but simultaneously undermines safety as a collision force. Cushioned shoes have been deemed to prevent lower extremity injuries caused by excessive vertical ground reaction force (vGRF). However, recent studies debunk this common belief, asserting that shoe hardness does not change the peak vGRF (PVGRF). This discrepancy is explained by the "muscle tuning" paradigm that the overall stiffness of the lower body including the shoes remains constant and spring-like function of the cushions offsets their own shock absorption capacity. This paper presents a novel shock-absorbing foot orthotic device capable of re-profiling the vGRF profile during landing. The proposed device is founded on two main hypotheses: change in the shoe hardness during landing can

modify (1) the vGRF profile and (2) the collision time. The foot-tailored, horseshoe bellows cushions are made through the layered manufacturing process and affixed to the bottom of commercial minimalist shoes. The proposed device identifies the phases of jump landing through sensors mounted under insoles and modulates the spring and damping coefficients of the cushions in compliance with those phases. The change in mechanical properties is realized by adjusting the airflow of the cushions. This paper conducted a preliminary experiment on one subject to evaluate the validity of the proposed device and compare it with that of three following commercial shoes: minimalist shoes (MINI), foam-cushioned shoes (FOAM), and air-cushioned shoes (AIR). The overall results substantiate the hypotheses, and also indicate that the proposed device has the best shock absorption capability. The proposed device exhibited the lowest vertical instantaneous loading rate (VILR) of all footwear conditions, which was 62%, 34%, and 24% lower than that of MINI, FOAM, and AIR, respectively. Likewise, its PVGRF was the lowest of all conditions, which was 22%, 17%, and 21% lower than that of MINI, FOAM, and AIR, respectively. This led to a slight decrease in the propulsion assistance, but a diminution in the collision force considerably surpassed that in the thrust force. The pushoff peak (POP), or maximum thrust force, of the proposed device was the lowest of all conditions, which was 3.1%, 5.8%, and 12% lower than that of MINI, FOAM, and AIR, respectively. However, the PVGRF to POP ratio (PVGRF/POP), or the landing impact at the same thrust force, of the proposed device was the lowest among all conditions, which was 20%, 11%, and 9.4% lower than that of MINI, FOAM, and AIR, respectively. This is accomplished by increase in the collision time and the ankle flexion moment. The collision time of the proposed device was the longest of all conditions, which was 12%, 17%, and 25% longer than that of MINI, FOAM, and AIR, respectively. Moreover, the proposed device aroused the largest ankle dorsiflexion during landing, which was 42%, 109%, and 124% larger than that of MINI, FOAM, and AIR, respectively. Nevertheless, the influence of the proposed device upon landing stability was analogous to that of

the other shoes. The landing time of the proposed device was 18% shorter than that of MINI, while 4% and 11% longer than that of FOAM and AIR, respectively. Meanwhile, its landing impulse was the smallest of all conditions, which was 14%, 4.9%, 2.1% smaller than that of MINI, FOAM, and AIR, respectively. Future work will involve reorganizing the proposed device into an untethered wearable system, testing with additional subjects, and validating its efficacy on strenuous sport activities.

Keyword : Shock Absorption, Foot Orthotic Device, vGRF profile, Cushion, Variable Stiffness, Pneumatic Actuator

Student Number : 2019-22678

Table of Contents

List of Figures

List of Tables

Chapter 1. Introduction

1.1. Research Background

Terrestrial locomotion, such as walking, running, and jumping, is essential for a human being to lead a life independently. These movements are established by a series of actions that a person pushes one's body against the ground and a corresponding reaction force pushes the person away from the ground. Accordingly, the greater the force a person exerts on the ground, the greater the thrust force becomes [1]. However, immoderate ground reaction force (GRF) may lead to high chance of lower extremity injuries [2]. Various sport activities, such as soccer, basketball, gymnastics, aerobic dance, and running, contain an airborne phase that ends up with a landing phase [3]. The landing phase is accompanied by a sudden rise of the GRF towards the human body. Hence, the GRF has a duality which contributes to the improvement of the human motor performance as a thrust force, but simultaneously undermines safety of the human being as a collision force.

Indeed, previous literature designated vertical ground reaction force (vGRF) and vertical loading rate (VLR) as the primary causes of anterior cruciate ligament injuries [4, 5] and lower limb stress fractures [6, 7], respectively. Moreover, 60 to 70 per 100,000 people annually suffer from meniscal injuries because the meniscus undergoes 20% of the landing impact [8]. In order to abate the lower extremity injuries derived from the vGRF, cushioned shoes have been widely used for decades. Earlier studies which applied an impact to a fixed leg supports the common belief that the GRF is strongly related to shoe hardness and soft shoes absorbs the landing impact better than hard shoes [9]. However, recent studies on runners and jumpers contradict the efficacy of the cushioned shoes, asserting that there are very small or no difference in peak vGRF between footwear conditions [10–12]. This discrepancy is explained by the “muscle tuning” paradigm that motion and stiffness of lower limbs depend on

a person's expectation about the landing surface [13]. Namely, the overall stiffness of the lower body, consisting of the human body and the landing surface, remains constant and spring-like function of a soft surface offsets its own shock absorption capacity [14, 15]. Shoes with constant stiffness function as the soft surface, herein precipitating the discrepancy in the cushioning effectiveness.

The concept of variable stiffness is already introduced to the fields of assistance and rehabilitation. A lateral wedge attached shoe [16, 17] and a shoe with medio-laterally asymmetric stiffness [18-21] reduce the knee adduction moment (KAM). Besides, prosthetic feet [22, 23] and an exoskeleton [24] with variable stiffness units assist disabled people in embodying a normative joint stiffness. However, these technologies do not address the vGRF, the primary source of the lower extremity injuries. Thus, there is a need for a foot orthotic device that can attenuate the vGRF with minimal disturbance to the locomotion.

1.2. Research Objectives and Contributions

Figure 1. Prototype of a shock-absorbing foot orthotic device using pneumatic variable stiffness actuators.

This paper presents a novel shock-absorbing foot orthotic device capable of re-profiling the vGRF profile during landing (Figure 1.). The foot-tailored, horseshoe bellows cushions are affixed to the bottom of commercial minimalist shoes. The proposed device identifies the phases of jump landing through sensors mounted under insoles and modulates the spring and damping coefficients of the cushions in compliance with those phases. The change in mechanical properties is realized by adjusting the airflow of the cushions. The proposed device affords slightly less propulsion assistance than the commercial shoes. Nonetheless, a diminution in the collision force considerably surpasses that in the thrust force. Furthermore, the influence of the proposed device upon landing stability is analogous to that of the common cushioned shoes.

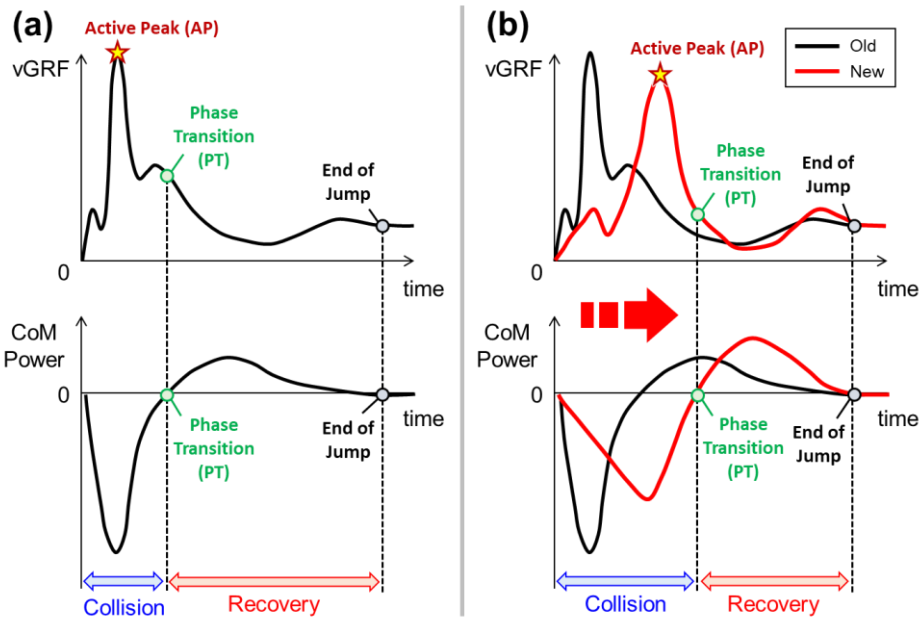

Figure 2. The vGRF and the center of mass (CoM) power profiles of (a) the common shoes and (b) the proposed device.

Two main hypotheses are formulated to develop the proposed device (Figure 2.).

Hypothesis I: If the spring and damping coefficients of the shoes change during landing, the vGRF profile shifts.

The proposed devise is assumed to maneuver the vGRF profile in right lower direction. This would lead to decrease in the peak vGRF and the VLR compared to the common shoes.

Hypothesis II: If the spring and damping coefficients of the shoes change during landing, the collision time varies.

The collision impulse ($I_{\text{Collision}}$) is assumed to remain constant irrespective of the footwear conditions.

$$I_{\text{Collision}} = \int_0^{t_{\text{Collision}}} F\, dt = \text{const.} \quad (1)$$

Accordingly, the proposed device would prolong the collision time ($t_{\text{Collision}}$) due to reduction of the peak vGRF.

Chapter 2. Methods

2.1. Mathematical Modelling

Nomenclature

m_1	the lower body rigid mass (LBRM) (kg)
m_2	the lower body wobbling mass (LBWM) (kg)
m_3	the upper body rigid mass (UBRM) (kg)
m_4	the upper body wobbling mass (UBWM) (kg)
k_1	the compressive spring connecting the UBRM and the LBRM (kN/m)
k_2	the spring connecting the LBRM and the LBWM (kN/m)
k_3	the spring connecting the UBRM and the LBWM (kN/m)
k_4	the spring representing the elastic properties of the contractile elements of the muscle–tendon units (kN/m)
k_5	the spring representing the serial elastic element in the muscle–tendon units (kN/m)
c_1	the damper connecting the UBRM and the LBRM (kg/s)
c_2	the damper connecting the UBRM and the LBWM (kg/s)
c_4	the damper representing the damping properties of the contractile elements of the muscle–tendon units (kg/s)
x_1	the vertical displacement of the LBRM (m)
x_2	the vertical displacement of the LBWM (m)
x_3	the vertical displacement of the UBRM (m)
v_1	the deformation velocity of the contact element (m/s)
F_g	the vertical contact force acting on the foot from the ground (N)
A_c	the ratio of the contact area during the ground contact to the area of the contact between foot and the impact pendulum (dimensionless)
a	the proportionality constant of the hardening spring of the shoe (N/m^b)

b	the position exponential constant of the hardening spring of the shoe (dimensionless)
c	the proportionality constant of the position−dependent damper of the shoe (N/m^{b}m^{e}s^e)
d	the position exponential constant of the position−dependent damper of the shoe (dimensionless)
e	the velocity exponential constant of the position−dependent damper of the shoe (dimensionless)
g	the gravity constant (m/s^2)
J_{fv}	the sum of force and vibration amplitude cost functions (dimensionless)
p_1	the first peak of the GRF (N)
p_2	the second peak of the GRF (N)
Λ	the vibration amplitude of the LBWM (m)

Subscripts

0	the initial value of variables
CoM	the center of mass (CoM) value of variables

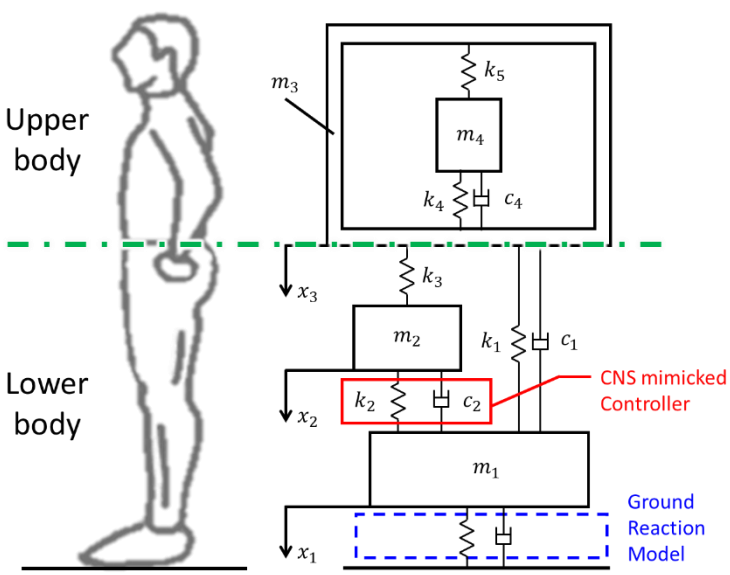

Figure 3. Schematic representation of the passive multi−body MSD model developed by Zadpoor and Nikooyan [27, 28].

The mass−spring−damper (MSD) modelling approach has been widely used to simulate the human musculoskeletal system during the locomotion, due to its simplicity. Among a variety of MSD models, the passive multi−body MSD model embodies simulation results closest to the actual experimental results [25]. This model describes the human body as a mechanical coupling of wobbling and rigid masses (Figure 3.).

The ground reaction model connects the human body to the ground. The vertical ground reaction force (vGRF) acting on the human body, F_g, is modelled as a function of the displacement (x_1) and velocity (v_1) of the lower body rigid mass (LBRM) [26]. The parameters and touchdown velocities of the ground reaction model are summarized in the following tables (Table 1., 2.).

$$F_g = \begin{cases} A_c\left[a x_1^{b} + c x_1^{d} v_1^{e}\right] & (x_1 > 0) \\ 0 & (x_1 \le 0) \end{cases} \tag{2}$$

Table 1. Parameters of the shoes.

	a	b (E_{shoe})	c	d (η_{shoe})	e
Default	0.6×10^6	1.38	2.0×10^4	0.75	1.0
Soft shoe		1.24		0.81	
Hard shoe		1.33		0.69	

Table 2. Touchdown velocities of the body masses.

	m_1	m_2	m_3	m_4
Touchdown velocities (m/s)	0.96		2.0	

However, the passive MSD models lose validity when the stiffness of soft tissues does not remain constant, as muscle activities during locomotion changes their stiffness. Therefore, Zadpoor and Nikooyan presented the modified passive multi−body MSD model (ZN model) by adding the central nervous system (CNS) mimicked controller. This controller adjusts stiffness (k_2) and damping (c_2) of

the lower body wobbling mass (LBWM) in compliance with the shoe hardness parameters (b and d). An excitation signal made by the controller, χ, modulates the mechanical properties of the human body (k_2 and c_2). Their model reflects the pre-landing activity of the lower limb muscles to compensate for the drawbacks of the passive models. The governing equations of motion are as follows [27, 28].

$$\begin{aligned}
m_1\ddot{x}_1 &= m_1 g - F_g - k_1(x_1 - x_3) - k_2\langle\chi\rangle(x_1 - x_2) - c_1(\dot{x}_1 - \dot{x}_3) \\
&\quad -c_2\langle\chi\rangle(\dot{x}_1 - \dot{x}_2) \\
m_2\ddot{x}_2 &= m_2 g + k_2\langle\chi\rangle(x_1 - x_2) - k_3(x_2 - x_3) + c_2\langle\chi\rangle(\dot{x}_1 - \dot{x}_2) \\
m_3\ddot{x}_3 &= m_3 g + k_1(x_1 - x_3) + k_3(x_2 - x_3) - (k_4 + k_5)(x_3 - x_4) + c_1(\dot{x}_1 - \dot{x}_3) \\
&\quad -c_4(\dot{x}_3 - \dot{x}_4) \\
m_4\ddot{x}_4 &= m_4 g + (k_4 + k_5)(x_3 - x_4) + c_4(\dot{x}_3 - \dot{x}_4)
\end{aligned} \tag{3}$$

The CNS mimicked controller intends to minimize the cost function (J_{fv}) that combines differences in force and vibration amplitude between a random shoe and the default value.

$$J_{fv} = \left(\left|\frac{p_1\langle b_i, d_i\rangle - p_{1,0}}{p_{1,0}}\right| + \left|\frac{p_2\langle b_i, d_i\rangle - p_{2,0}}{p_{2,0}}\right|\right) + \left|\frac{\Lambda_i\langle b_i, d_i\rangle - \Lambda_0}{\Lambda_0}\right| \tag{4}$$

The ZN model anticipates that the vGRF profile remains constant only when spring (b) and damping (d) coefficients of the shoe are within the "safe region." In other words, the vGRF profile would change if a person wears a shoe whose hardness lies outside the safe region (Figure 4. (a)). For instance, a hard shoe shows lower early peak and higher active peak than the default value. A soft shoe, on the other hand, shows higher early peak and lower active peak than the default value. The early peak (first peak) and the active peak (second peak; peak vGRF) correspond to a forefoot strike and a heel strike, respectively. In a nutshell, a shoe with constant stiffness has both merits and demerits.

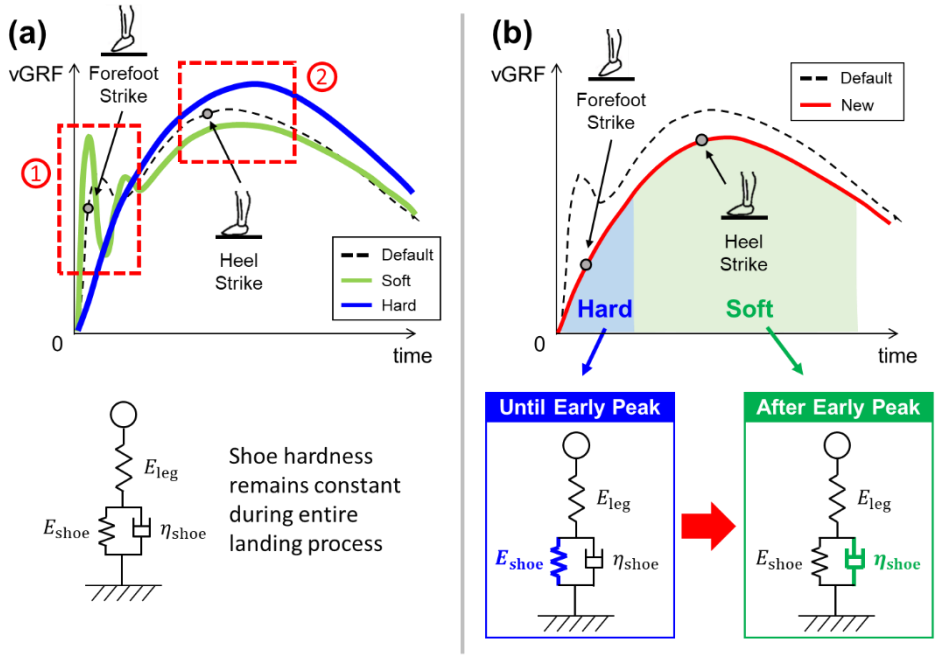

Figure 4. (a) The vGRF profiles of the shoes with constant stiffness predicted by the ZN model [28].
(b) The expected vGRF profile of the proposed device.

This paper supposes that the variable stiffness cushion can alter the vGRF profile by tailoring its mechanical properties in line with the jump landing phases. (Hypothesis I) After the touchdown, it initiates as the "hard" shoe and then transits to the "soft" shoe following the forefoot strike (Figure 4. (b)). This operating sequence enables the device to combine the advantages of the soft and hard shoes while also excluding their disadvantages. The new vGRF profile described in the previous chapter (Figure 2.) may be realized by the proposed device. Since the collision impulse remains constant regardless of footwear conditions, the new profile implies that the collision time will increase as the active peak decreases. (Hypothesis II)

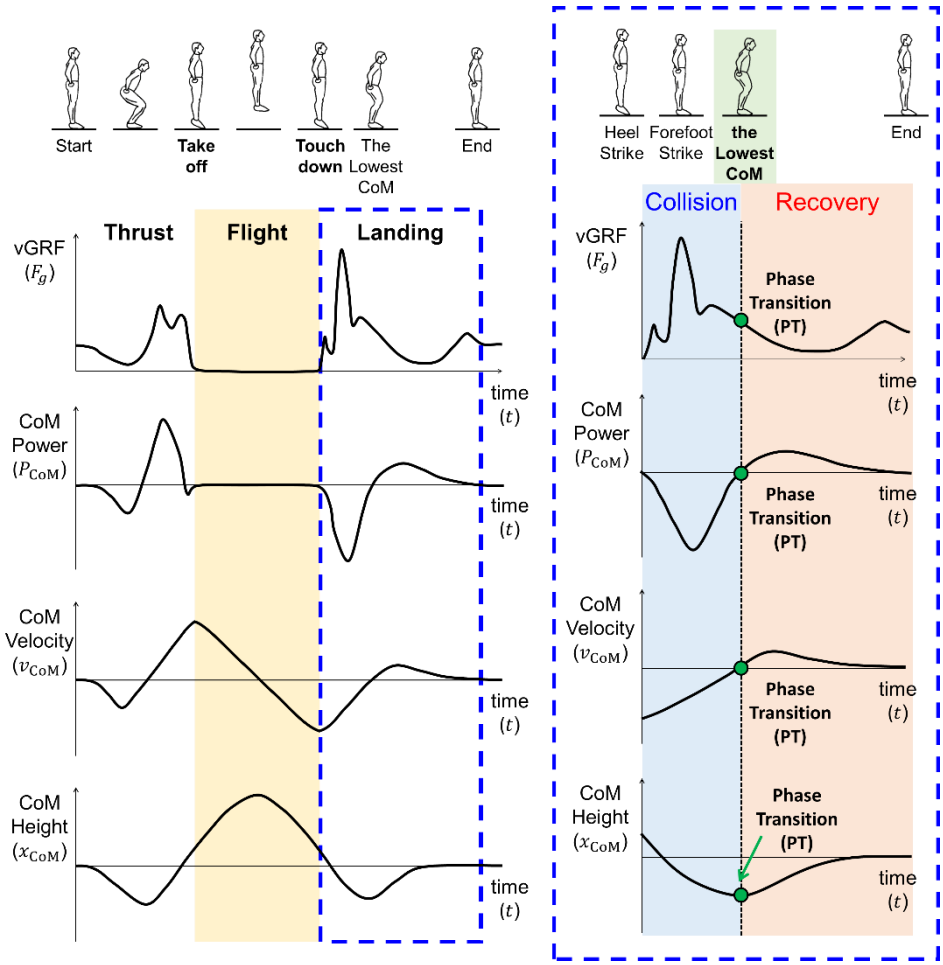

Figure 5. The vGRF, CoM power, CoM velocity, and CoM height profiles during the vertical countermovement jump.

In order to corroborate the change in the collision time (Hypothesis II), profound understanding of the landing process is needed. The landing process consists of two phases in terms of work direction: collision and recovery (Figure 5.). People conduct negative work to banish the kinetic energy gained from the descent during collision phase. On the other hand, people conduct positive work to return to the standing rest posture during recovery phase [29]. Meanwhile, the phase transition (PT) point, at which the CoM power is zero, indicates that the CoM velocity is also zero (Equation. (5)). In other words, the CoM reaches the lowest point at the PT point, leading to its maximum vertical displacement. Since the collision time

equals to the duration from the touchdown to the PT point, it would increase as the time to the lowest CoM point increases.

$$P_{\mathrm{CoM}} = F_g \cdot v_{\mathrm{CoM}} \tag{5}$$

$$\text{where } v_{\mathrm{CoM}}(t) = \int_{t_{\mathrm{Start}}}^{t} a_{\mathrm{CoM}}\, dt = \int_{t_{\mathrm{Start}}}^{t} \frac{1}{m}\left(F_g - mg\right) dt$$

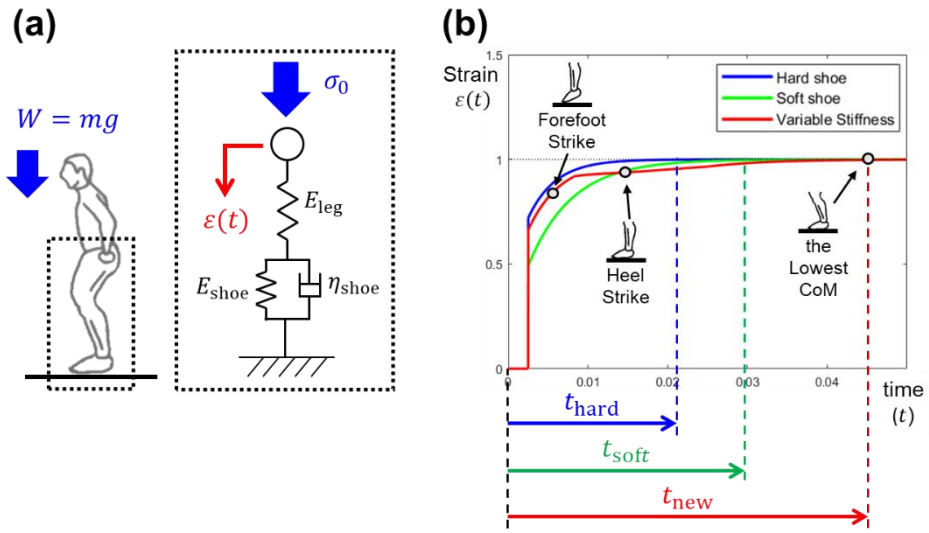

Figure 6. (a) The simple one-body modelling of landing. (b) The relationship between strain and time during the collision phase.

Previous literature analyzed that the entire landing process is completed within 2 seconds and the active peak occurs within 0.05 seconds after the touchdown [30, 31]. Thus, the impact during collision phase can be considered as a sudden stress (σ_0) and the relationship between strain (ε) and time (t) can be predicted using a creep characteristic (Figure 6. (a)). The strain represents the relative vertical displacement of the CoM. Hence, when the strain attains the maximum value, the CoM reaches the lowest point.

$$\varepsilon(t) = \sigma_0 \cdot J(t) = J_0\left[1 + q_1\left\{1 - exp\left(-\frac{t}{\tau}\right)\right\}\right] \tag{6}$$

$$\text{where } J_0 = \frac{1}{E_{\mathrm{leg}}},\ q_1 = \frac{E_{\mathrm{leg}}}{E_{\mathrm{shoe}}},\ \tau = \frac{\eta_{\mathrm{shoe}}}{E_{\mathrm{shoe}}}$$

The values in Table 1. were utilized to simulate the collision time of each footwear condition. The simulation predicts that the time to the lowest CoM point of the variable stiffness cushion is longer than that of the soft and hard shoes (Figure 6. (b)). Consequently, the proposed device will have longer collision time than the shoes with constant stiffness, matching the implication of the new vGRF profile. (Hypothesis II)

2.2. Actuator Design

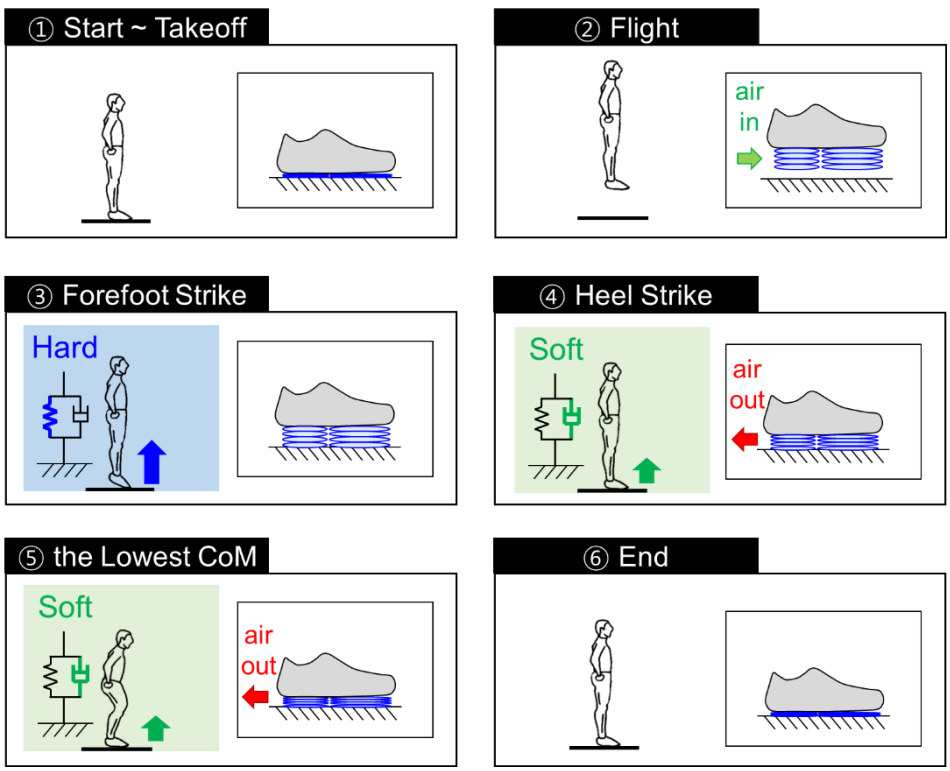

Figure 7. Operating sequence of the proposed device.

The control of airflow alongside the jump landing modifies the mechanical properties of the proposed device. The cushion remains flat until the takeoff. During the flight phase, an air inlet is opened and the cushion expands to a preassigned pressure. After the touchdown, both inlet and outlet are closed to maintain the stiffness

of cushion. This results in the "hard" cushion and continues until the forefoot strike is over. Then, the air outlet is opened and the cushion begins deflating by the landing impact and body weight. This leads to the "soft" cushion and continues until the cushion becomes flat (Figure 7.). This operating sequence makes the human body decelerate slowly, resulting in longer collision time than the shoes with constant stiffness.

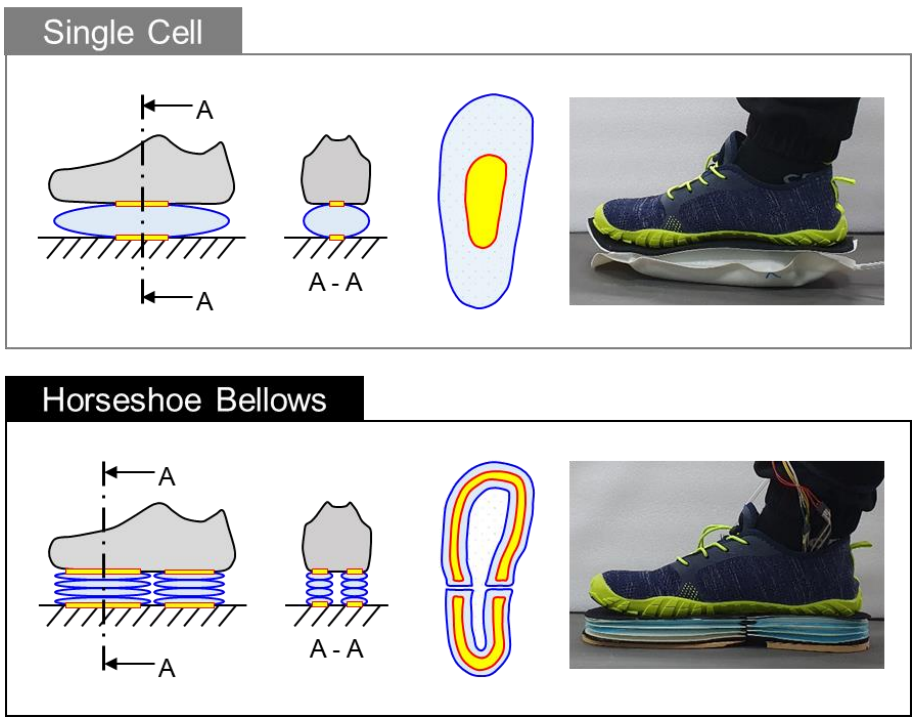

Figure 8. Design comparison of the single cell and the horseshoe bellows cushions.

The proposed device adopts a horseshoe bellows design to increase stability and efficiency compared to a single cell structure (Figure 8.). First, the horseshoe design enhances the stability. A ground contact area of single cell is biased to the center, making it difficult to keep balance when worn. Accordingly, the cushion should enclose the foot shape to maximize the ground contact area and prevent the imbalance during landing. Next, the bellows design improves the efficiency. Previous studies found that effectiveness of

shock absorption relies on the maximum vertical displacement of the CoM [11, 14, 15]. The bellows design can generate the higher cushion with same volume of air than the single cell design, since the single cell chamber inflates in all directions while the bellows chamber primarily inflates in a stacked direction. Additionally, flight and landing period ends in less than 0.5 and 2 seconds, respectively [30, 31]. Thus, the bellows design is preferable to the single cell design in order to ensure sufficient time for inflation and deflation.

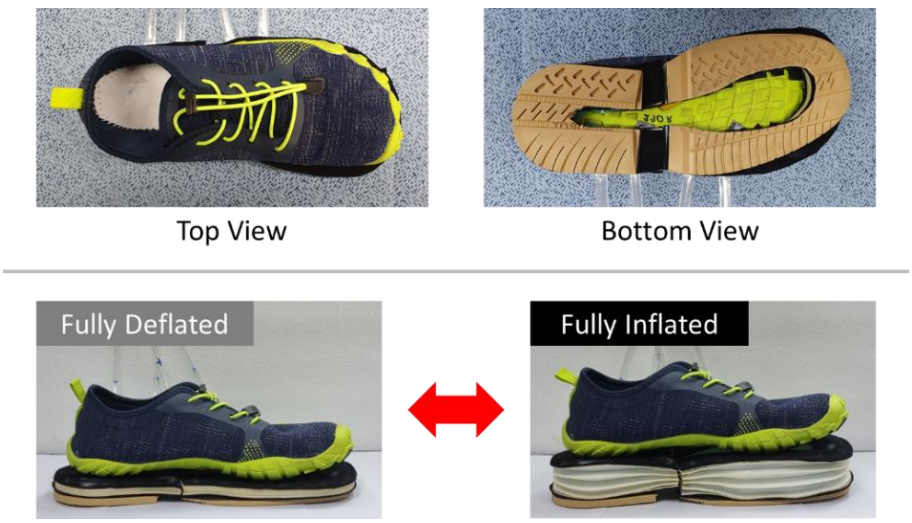

Figure 9. Overview of the minimalist shoes with the horseshoe bellows cushions.

The variable stiffness cushion is originally designed as an auxiliary device that can be adhered to the other shoes, such as crampons and snowshoes. It is attached underneath typical shoes via velcro® and an additional outsole (XA-7 424 Outdoor; Michelin SCA, Clermont-Ferrand, France) is attached below the cushion to enhance the grip force. In this study, the horseshoe bellows cushion is affixed to the minimalist shoes (TF-BK40; Tesla Gear, Paju-si, Gyeonggi-do, Republic of Korea) to construct the system. These shoes have minimal cushions and resembles the shape of a person's feet, making them a desirable framework for the proposed device (Figure 9.).

Besides, the system is divided into forefoot and heel cushions in

order to conform with foot strike pattern: forefoot strike first, then heel strike. The controlling mechanism can be altered to attune forefoot and heel cushions individually, even though the cushions operate simultaneously in this paper. This additional operating mode may accommodate sport activities that require faster response than walking and jumping.

Moreover, the cushion consists of four chambers in order to match the cushion height of the control group. The air-cushioned shoes (Air Max Excellerate 4; Nike Inc., Beaverton, OR, USA) and foam-cushioned shoes (Royal Aadorun; Reebok International. Ltd., Boston, MA, USA) have 45 mm and 42 mm high cushions, respectively. In the meantime, the horseshoe bellows cushion is 8 mm high under fully deflated and 30 mm high under fully inflated. The cushion height of the proposed device, the sum of the variable stiffness cushion and the outsoles, ranges from 15 mm to 37 mm, comparable with the control group.

2.3. Manufacturing Process

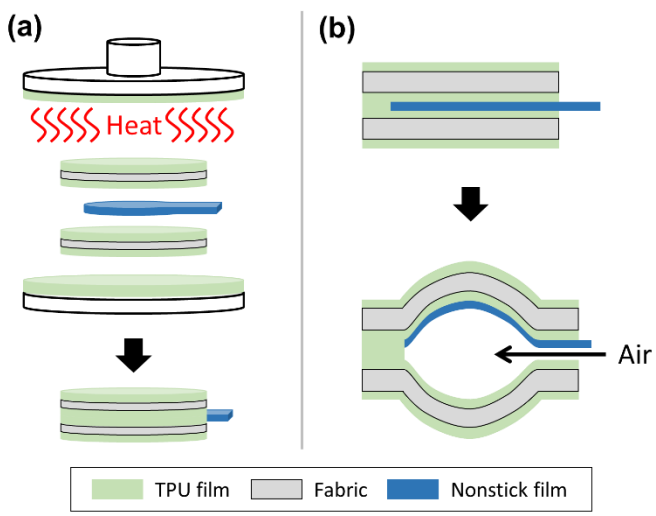

Figure 10. (a) Schematic representation of the layered manufacturing process.
(b) Diagram of a single chambered inflatable structures made by the aforementioned process.

Pneumatic variable stiffness actuators, or the variable stiffness cushions, are airtight, unitary, and multi-chambered inflatable structures. The actuators should be flexible and flat to minimize interference with the wearer during the thrust and recovery phase, but they should be able to expand significantly in the vertical direction to secure sufficient vertical displacement during the collision phase. This study applies the layered manufacturing method presented by Yang and Asbeck to create the actuators that satisfy the aforementioned prerequisite. Their method can produce multi-chambered inflatable structures with layers of textiles and thermal adhesive film [32].

This paper applies their approach with nonstick release films (Wrightlon 5200; Airtech International. Inc., Huntington Beach, CA, USA) and fabrics coated with thermoplastic poly-urethane (TPU) films on both sides (Polyester nonwoven fabric coated with TPU; Jiaxing Inch Eco Materials Co., Jiaxing, Zhejiang, China). When two TPU-coated fabrics are placed in the heat press (QM900A; Qmesys, Uiwang-si, Gyeonggi-do, Republic of Korea) and the heat press is clamped down, the fabrics receive high heat, TPU films facing each other melt, and the fabrics are bonded together. However, if the nonstick films are placed between the TPU films, TPU films do not adhere to each other. The heat press is covered with the nonstick films to prevent bonding between the heat press and the structure (Figure 10.).

The horseshoe bellows cushion is produced through a series of fabricating steps (Figure 11.). First, the minimalist shoes are scanned to design a cushion shape. Second, the scanned picture is transformed into a blueprint via a CAD program (SOLIDWORKS; Dassault Systèmes SolidWorks Co., Waltham, MA, USA). The blueprint is divided into two parts: forefoot and heel cushions. Third, TPU-coated fabrics and nonstick films are cut to the blueprint with a 60W CO_2 laser (VLS 3.50; Universal Laser Systems Inc., Scottsdale, AZ, USA). The CO_2 laser is set to 20% speed, 80% power, and 500 pulses per inch for TPU-coated fabrics. On the other hand, it is set to 80% speed, 10% power, and 500 pulses per inch for nonstick films.

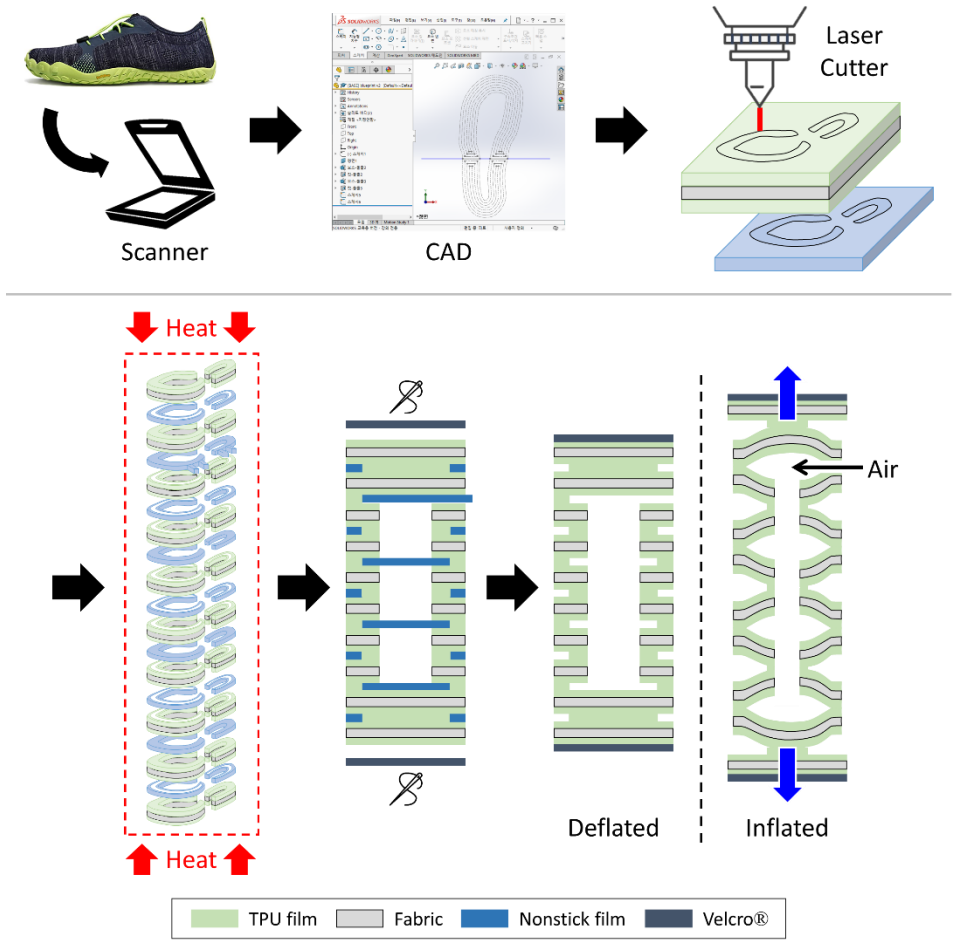

Figure 11. Manufacturing process of the horseshoe bellows cushion.

Fourth, the patterned TPU-coated fabrics and nonstick films are stacked manually and placed in the heat press at 165℃ for 60 minutes. This setting is just above the melting point of the TPU-coated fabrics. After the first 30 minutes, the heat press was opened, the structure was rotated 90 degrees, and then the heat press was clamped down for another 30 minutes. Then, the heater is turned off and the structure remains pressed until the temperature of the heat press cools below 70℃. This procedure enables uniform bonding throughout the structure. Fifth, velcro® fabrics are sewn to the top and bottom of the structure through a sewing machine (DDL-9000C-FMS; JUKI Co., Tama, Tokyo, Japan). In addition, air tubes are inserted into the structure to create air inlet and outlet. To

minimize air leakage due to gaps between the air tubes and the structure, the air tubes are flattened in the heat press at 165℃ for 5 seconds. The remaining gaps are filled with teflon® tapes and adhesives. Finally, the finished horseshoe bellows cushion maintains flexibility and flatness during the deflated state, but greatly expands in the vertical direction during the inflated state.

2.4. System Integration

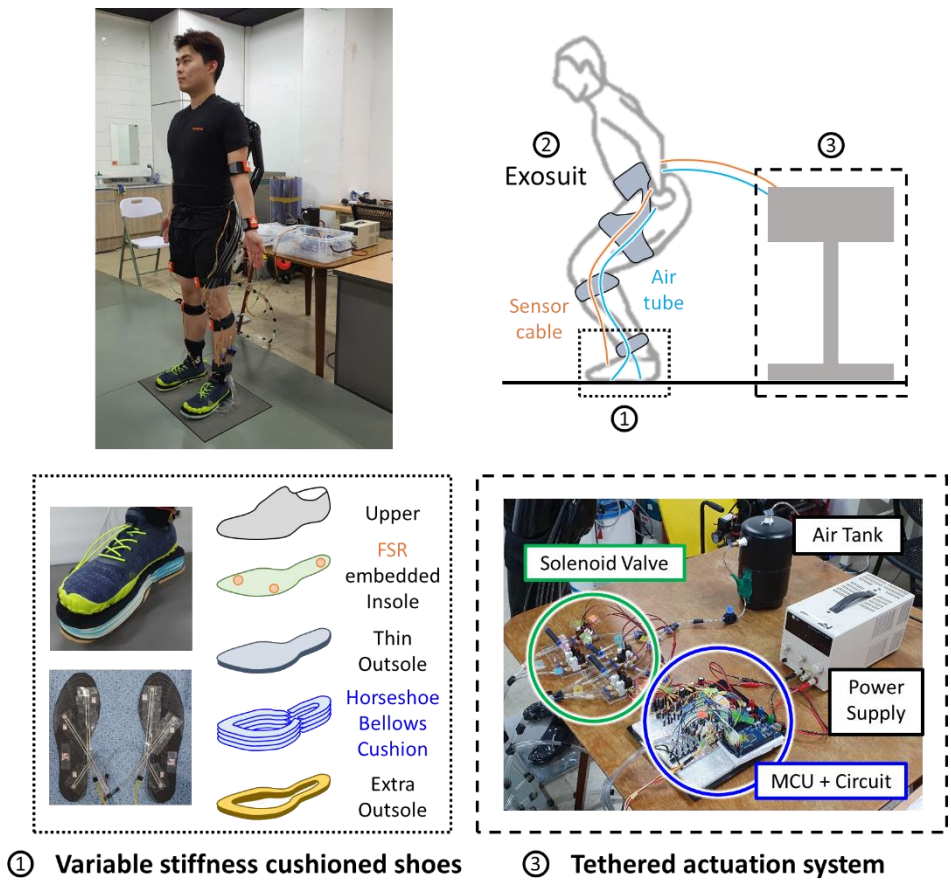

Figure 12. Overview of the integrated system.

The complete system consists of three main components: variable stiffness cushioned shoes, exosuit, and tethered actuation system (Figure 12.). First, the cushioned shoes comprise the

minimalist shoes, forefoot and heel horseshoe bellows cushions, force sensing resistor (FSR) sensor embedded insoles, and extra outsoles. Three FSR sensors (FlexiForce A201-25; Tekscan Inc., Boston, MA, USA) are placed under heel, fifth metatarsal, and hallux of each insole to detect the ground contact.

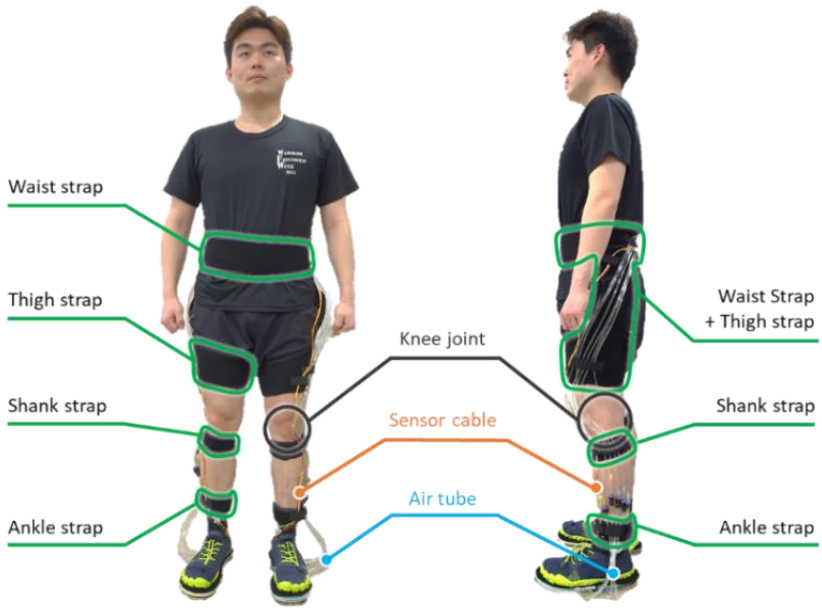

Figure 13. Arrangement of the exosuit in the integrated system.

Table 3. Mass of the integrated system except the tethered actuation system.

Components	Mass (g)
Minimalist Shoes	563
Extra Outsoles	205
Horseshoe Bellows Cushions	295
FSR embedded insoles	68
Exosuit (straps with wiring paths)	362
Sensor Cables and Air Tubes	348
Total	1841

Second, the exosuit consists of straps with wiring paths to place sensor cables and air tubes close to the body and prevent them from fluttering during vertical jumps. The straps are made of neoprene and located on the waist, thighs, shanks and ankles (Figure 13.). Each strap can easily change its perimeter through velcro® to correspond with an individual body type. To restrict the thigh straps from sliding, they are connected to the waist strap via velcro®. The mass of the integrated system except the tethered actuation system, which is worn by the wearer is as above (Table 3.).

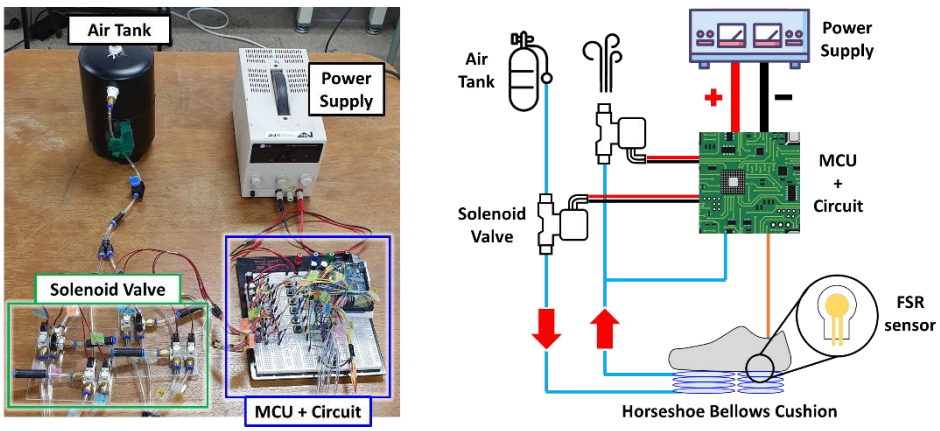

Figure 14. Overview of the tethered actuation system.

Third, the tethered actuation system consists of an air tank, a DC power supply, solenoid valves, an MCU, and a circuit (Figure 14.). The air tank (MS-TANK001; AirFactory Co., Seoul, Republic of Korea) with 4 atm of compressed air supplies air to the device. Two solenoid valves (UV280; Shinyeong Mechatronics, Siheung-si, Gyeonggi-do, Republic of Korea) per each cushion are used to adjust the airflow and mechanical properties of the proposed device. In addition, one barometer (33A-150G-2210; Shiba Korea Co. Ltd., Anyang-si, Gyeonggi-do, Republic of Korea) per each cushion is connected to an outflow tube to measure its pressure. Lastly, the MCU (Arduino MEGA 2560 rev3) controls the solenoid valves by data collected from the FSR sensors and the barometers. Further details of the control mechanism will be discussed in the next section.

2.5. Control Mechanism

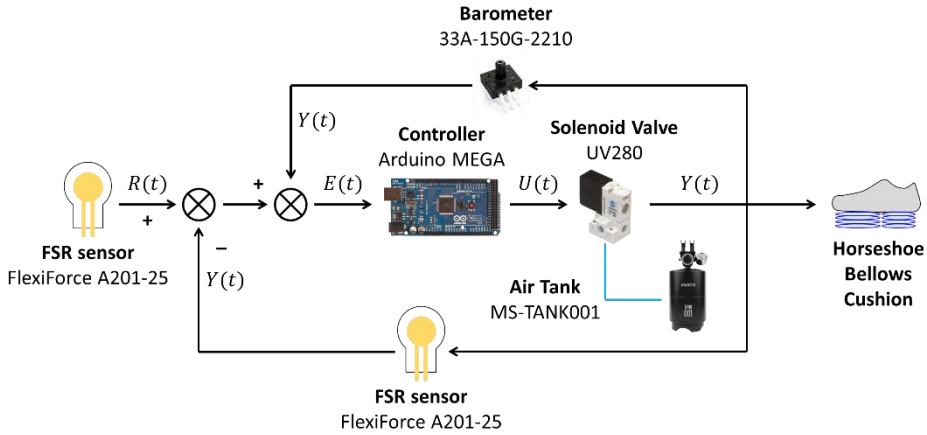

Figure 15. Schematic block diagram of the control mechanism.

A number of electronics are required to detect phases and attune the shoe hardness during the vertical jumps (Figure 15.). The contact with the ground is determined by the change in conductance of the FSR sensors ($G_{\mathrm{FSR}} = 1/R_{\mathrm{FSR}}$). Three FSR sensors ($FSR_{\mathrm{hallux}}$, FSR_{5met}, FSR_{heel}) are adhered below each insole and each sensor has different conductance profile during the vertical countermovement jump (Figure 16.). Two conductance thresholds are set to distinguish between the flight phase and the thrust phase: a flight threshold ($\mathrm{thld}_{\mathrm{flight}}$) and a contact threshold ($\mathrm{thld}_{\mathrm{contact}}$). When conductance of all FSR sensors are lower than the flight threshold ($\mathrm{thld}_{\mathrm{flight}}$), the wearer is considered to be in the flight phase. On the other hand, the wearer is considered to be in the ground contact phases – either thrust phase or landing phase – if any of the FSR sensors has higher conductance than the contact threshold ($\mathrm{thld}_{\mathrm{contact}}$).

Next, the MCU attunes the spring and damping coefficients of the proposed device according to the jump landing phases. The cushion remains "hard" from the touchdown to the end of the forefoot strike. Since a computing speed of the MCU is too slow to differentiate between the forefoot strike and the heel strike via the FSR sensors, this study supposes that the forefoot strike ends 0.04

seconds after from the touchdown [31]. After the preassigned time, the outflow valve is opened and the cushion becomes "soft".

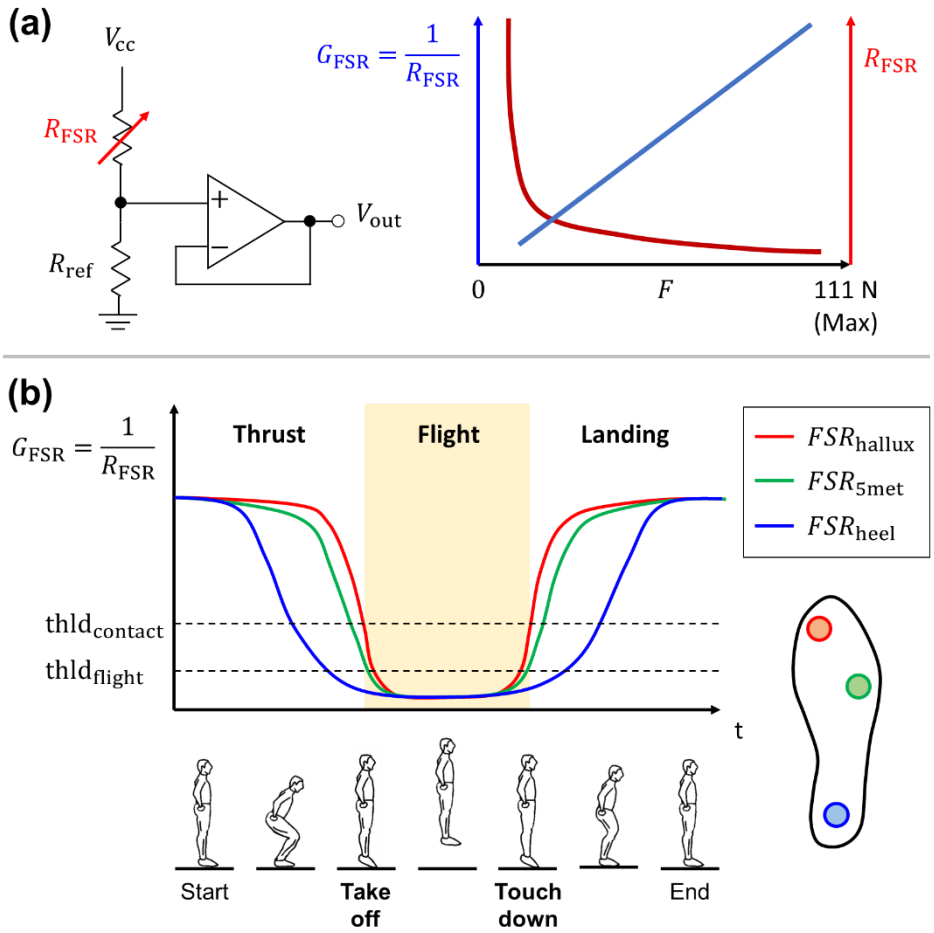

Figure 16. (a) Conductance and resistance characteristics of the FSR sensor vs. Compressive force.
(b) Conductance profiles of the FSR sensors during the vertical countermovement jump.

During the flight phase, an inflow valve is opened and the cushion is inflated to a preassigned pressure of 20 kPa (gauge pressure). The MCU checks the cushion pressure via the barometer and attains the desired pressure by controlling the inflow and the outflow valves. An allowable error is ±1 kPa and one barometer functions as a reference barometer to measure an ambient pressure. The barometer in each

cushion is calibrated on the basis of the reference barometer value.

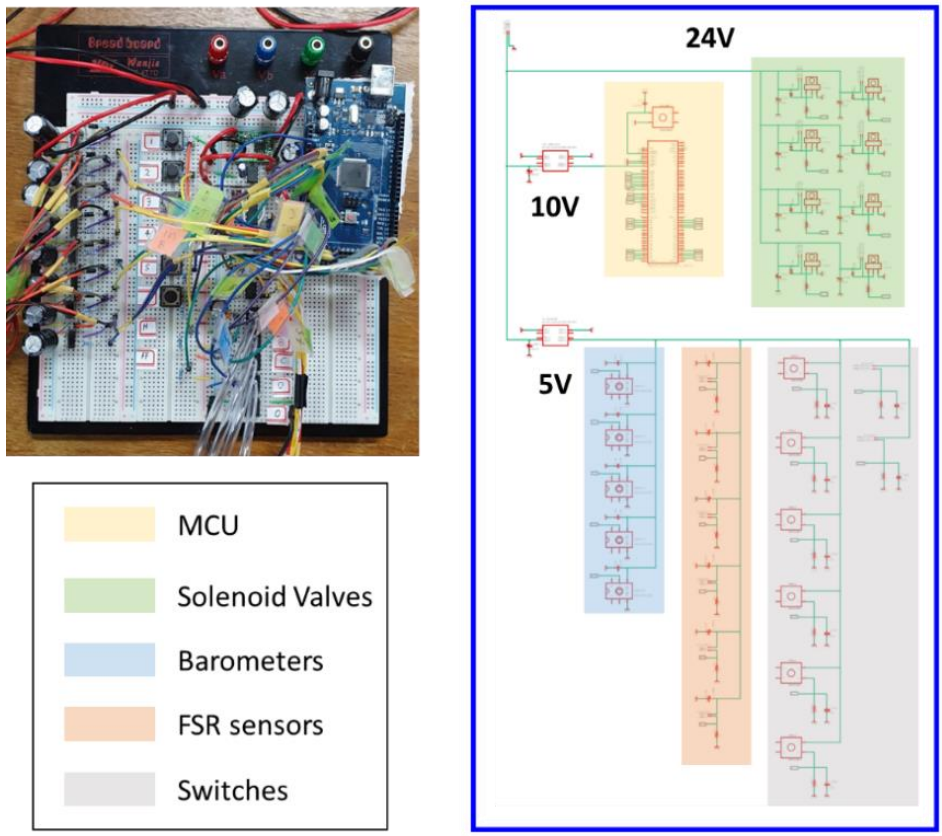

Figure 17. Circuit diagram of the tethered actuation system.

In short, the MCU detects the jump landing phases via the FSR sensors, measures the cushion pressure with the barometers, and modulates the shoe hardness through the solenoid valves. The tact switches are inserted into the circuit to alter the operating mode of the proposed device, such as the cushions operate individually, although these extra modes are not used in this study (Figure 17.).

2.6. Experimental Setup and Protocol

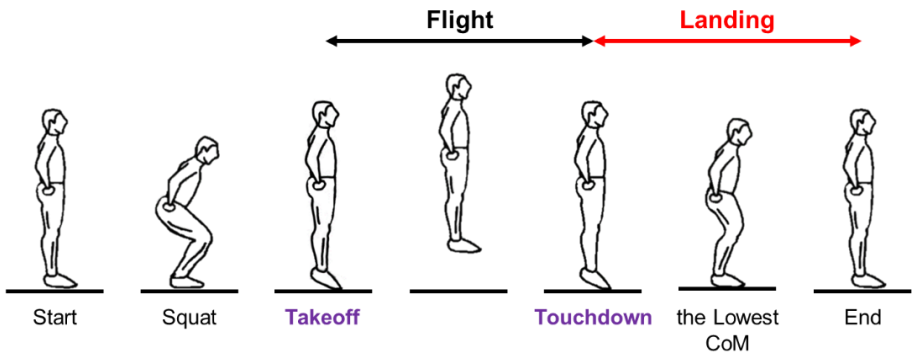

Figure 18. Sequence of the vertical countermovement jump.

This study conducted a preliminary experiment on one subject to evaluate the efficacy of the proposed device. The subject was requested to carry out consecutive jump (CJ) tasks. For each task, the subject performed a vertical countermovement jump every 5 seconds for 2 minutes (Figure 18.). The CJ task was repeated twice per each footwear condition. Specifically, the subject jumped as high as possible using one's lower limbs, following auditory signals from a metronome. At least 10 minutes of rest was provided between each task. In order to maintain a similar landing posture for each footwear condition, the subject was instructed to perform stiff landing. The stiff landing is a landing method in which maximum knee bending angle is less than 90 degrees from full extension [33]. After the touchdown, the subject was asked to return to the standing rest posture as soon as possible. A jump was considered valid if the subject landed with both feet on a force plate and did not lose the balance during landing. Moreover, the subject kept hands at one's waist, straightened back, and looked forward throughout the task. The physical properties of the subject are as follows (Table 4.).

Table 4. Physical properties of the subject.

	Age (years)	Height (m)	Body Mass (kg)	Shoe Size (mm)
Subject A	26	1.72	74.3	265

Figure 19. Footwear conditions used in the experiment.

The experiment was conducted with four different footwear conditions: the minimalist shoes (MINI), the foam-cushioned shoes (FOAM), the air-cushioned shoes (AIR), and the proposed device (NEW) (Figure 19.). The proposed device is the variable stiffness cushioned shoes based on the minimalist shoes (MINI). It converts its mechanical properties from "hard" to "soft", depending on the landing process. The subject practiced as many jumps as needed to familiarize with each footwear condition before actual measurements. The order of the conditions was as follows: NEW, AIR, FOAM, and MINI.

2.7. Data Collection and Reduction

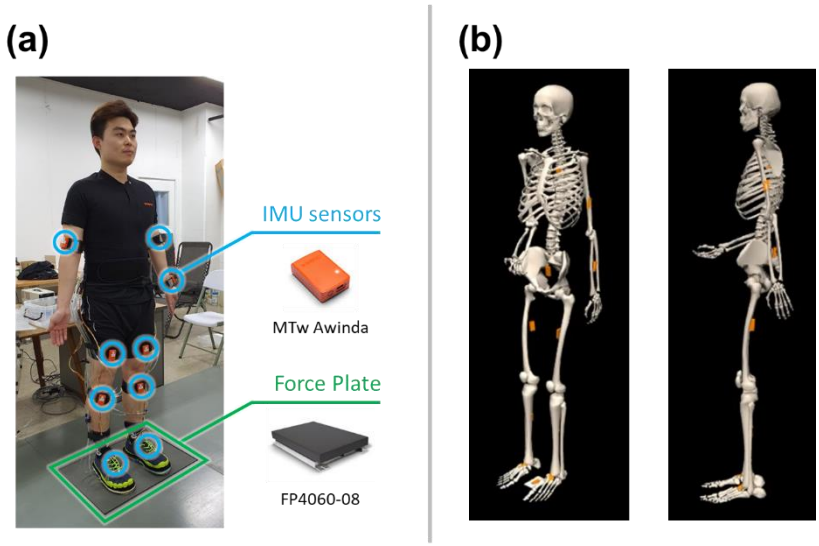

Figure 20. (a) Schematic representation of the experimental setup. (b) Motion tracking data processed by OpenSim.

Kinetic and kinematic data of the subject were collected through a force plate and IMU sensors, respectively (Figure 20. (a)). The subject fulfilled the experiment over the force plate (Bertec FP-4060-08; Bertec Corp., Columbus, OH, USA), which collected the vGRF (F_g) data at a frequency of 1000 Hz. In addition, 11 IMU sensors (MTw Awinda; Xsens Technologies B.V., Enschede, the Netherlands) were attached to the subject's body, collecting joint angle data at 60 Hz [34]. 8 sensors were placed bilaterally on the foot (calcaneus), shank (tibia), thigh (femur), and upper arm (humerus). The other three sensors were placed on the waist (pelvis), middle of the shoulder blades, left forearm (radius). Besides, one IMU sensor was placed on the platform (gray colored) to calibrate the sensors on the subject's body. The force plate and IMU sensors were time-synchronized through a master sync station and a software (myoSYNC and myoResearch 3.16; Noraxon U.S.A. Inc., Scottsdale, AZ, USA) during the experiment.

The data were analyzed using a customized MATLAB code

(v2020b; The Mathworks Inc., Natick, MA, USA) and neither kinetic nor kinematic data were filtered to avoid potential error [35]. The IMU sensor data were first converted into a motion file via OpenSim (v4.1; SimTK.org), from which the joint angle data were extracted (Figure 20. (b)) [36]. Then, the joint angle data were interpolated to coincide with the sampling frequency of the force plate data.

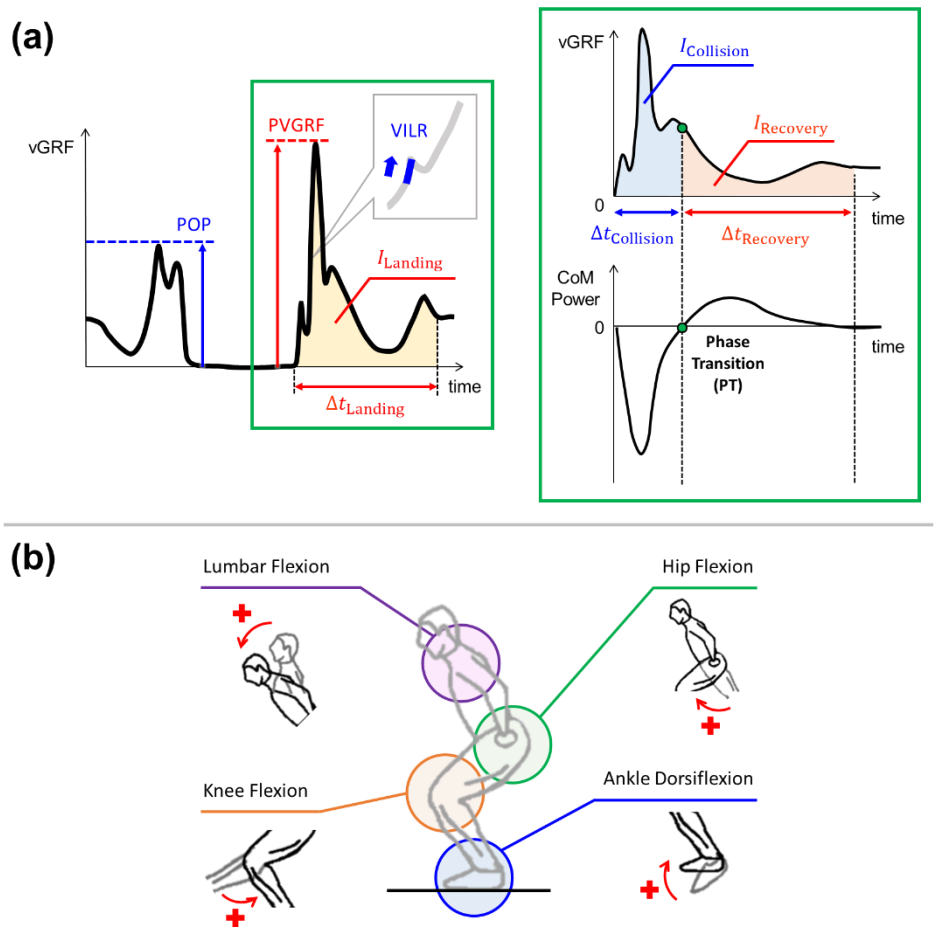

Figure 21. Evaluation metrics of the footwear conditions: (a) kinetic and (b) kinematic data

Before starting each CJ task, the subject was requested to stand upright with one's arms straight and palms facing forward for 5 seconds (Figure 20. (a)). The body weight (BW) of the subject was calculated by the average vGRF value during this period. Additionally,

IMU sensor data during this period were used to calibrate an OpenSim musculoskeletal model [37]. If the vGRF becomes less than and greater than 5 N during the jump landing, it is determined to be the moments of takeoff and touchdown, respectively. This threshold was designated based on the maximum error of the force plate while unloaded. Then, the touchdown is defined as 0 second on the time axis. The CoM power was computed as Equation. (5), where the CoM velocity was computed through numerical integration using the trapezoidal rule. Likewise, the impulse during landing means the area under the vGRF profile and was calculated via numerical integration as follows.

$$I_t = \int_{t_{\text{Touchdown}}}^{t} F_g \, dt = \int_0^t F_g \, dt \tag{7}$$

The vGRF, CoM power, and impulse data were normalized by the body weight. Besides, the end of jump is identified as the point where the CoM power is zero for the second time during landing (Figure 21.). The subject completely stops the locomotion at this point since the CoM velocity reaches zero and the vGRF equals to the body weight.

In order to evaluate the proposed device and compare it with the other footwear conditions, several evaluation metrics were defined based on the previous research (Figure 21.). First, a change in the vGRF profile is assessed through the force plate data. The goal of this paper is to verify that the proposed device reduces the peak vGRF and increases the collision time while not considerably increasing the landing time. (Hypothesis II) Second, the shock absorption is evaluated by three following metrics: VILR, PVGRF, and collision time ($\Delta t_{\text{Collision}}$). Vertical instantaneous loading rate, or VILR, indicates the maximum slope of the vGRF profile between the touchdown and the active peak [38, 39].

$$\text{VILR} = \max \frac{dF_g}{dt} \quad \text{where} \quad 0 < t < t_{\text{Active Peak}} \tag{8}$$

Peak vertical GRF, or PVGRF, means the vGRF value of the active peak. Meanwhile, pushoff peak, or POP, is the maximum vGRF value during the thrust phase and is used to calculate the maximum thrust force with each footwear condition. Collision time implies the effect of each shoe on the vGRF profile. (Hypothesis II) Third, the landing stability is appraised by the landing time ($\Delta t_{\mathrm{Landing}}$), which indicates the duration of the landing process or time from the touchdown to the end of jump. Lastly, a kinematic influence of each footwear condition is analyzed through following joint angles: lumbar flexion, hip flexion, knee flexion, and ankle dorsiflexion.

Chapter 3. Results

3.1. vGRF Profile

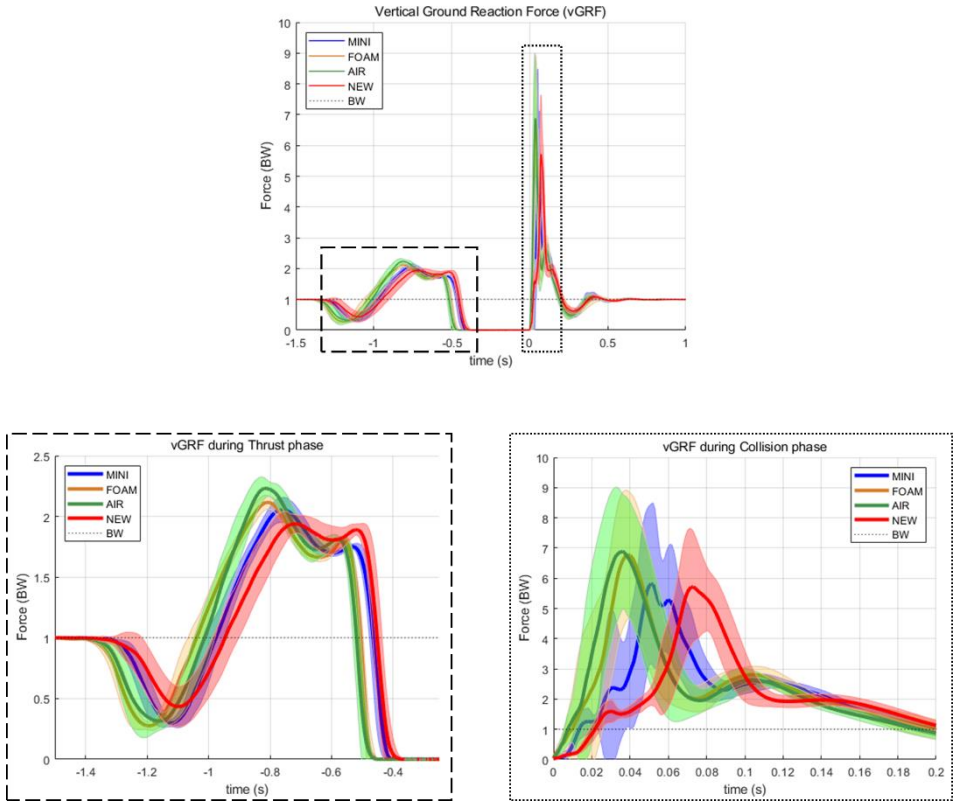

Figure 22. The vGRF profiles of all footwear conditions during the vertical countermovement jump. The solid blue, orange, green, and red lines represent the mean vGRF of MINI, FOAM, AIR, and NEW, respectively.

The vGRF profiles shifted according to the footwear conditions (Figure 22.). FOAM and AIR manifested analogous profiles in both thrust and collision phases. They had higher pushoff peak and active peak than MINI and NEW. Furthermore, their active peaks occur earlier than MINI. In the meantime, NEW exhibited a comparable profile to MINI during the thrust phase, but its active peak was smaller and occurred later than MINI in the collision phase. Namely,

the proposed device operates as MINI and does not significantly affect the wearer before the flight phase, whereas alters the vGRF profile by tailoring its mechanical properties during landing. (Hypothesis I)

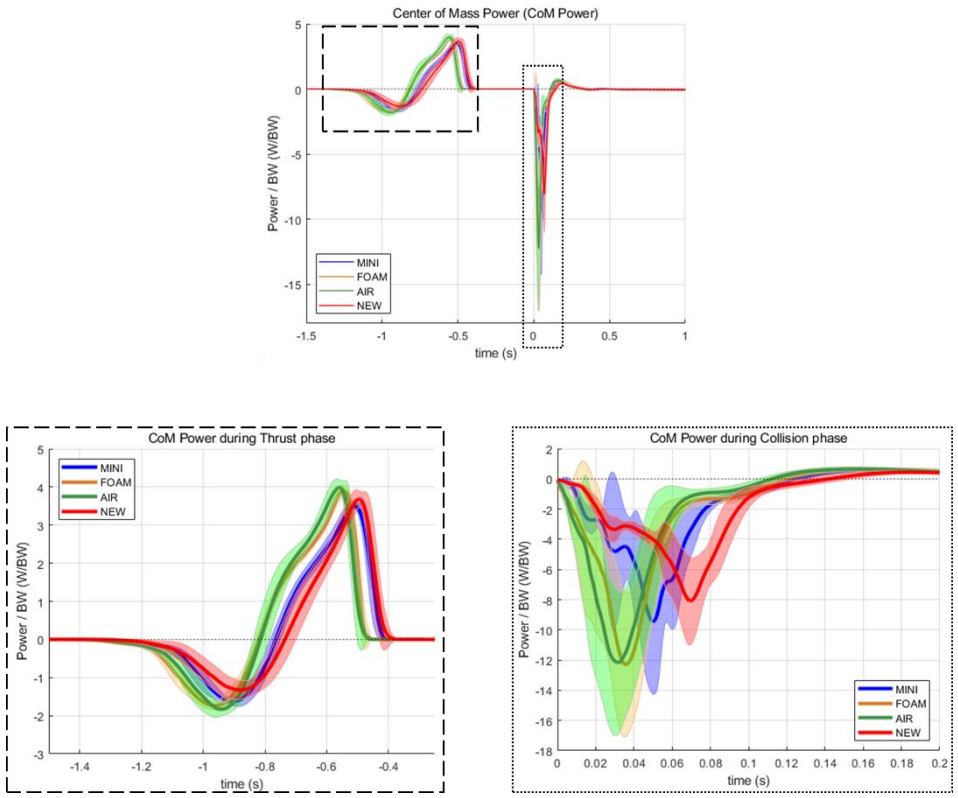

Figure 23. The CoM power profiles of all footwear conditions during the vertical countermovement jump. The solid blue, orange, green, and red lines represent the mean CoM power of MINI, FOAM, AIR, and NEW, respectively.

Likewise, the CoM power profiles were determined in accordance with the footwear conditions. During the thrust phase, FOAM and NEW showed similar profiles, which differed from MINI and NEW. The proposed device illustrated the latest and shallowest trough among all conditions during landing.

3.2. Shock Absorption

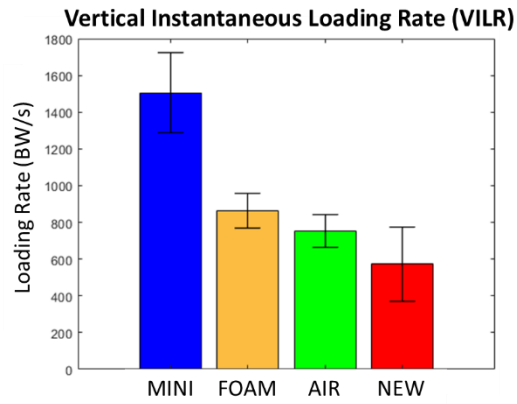

Figure 24. Vertical instantaneous loading rates (VILRs) of all footwear conditions. The blue, orange, green, and red bars represent MINI, FOAM, AIR, and NEW, respectively.

First, the vertical instantaneous loading rates (VILR) is often designated as the primary cause of the lower extremity stress fractures [6, 7, 38]. Therefore, a shoe with low VILR has high shock absorption performance. The proposed device displayed the lowest VILR of all footwear conditions, which was 62%, 34%, and 24% lower than that of MINI, FOAM, and AIR, respectively (Figure 24.).

Next, the pushoff peak (POP) and peak vGRF (PVGRF) indicate the maximum thrust force and the maximum collision force, respectively. Accordingly, a shoe with high POP has substantial propulsion assistance during jumping. Conversely, a shoe with low PVGRF has high shock absorption performance during landing. Hence, it is essential to control the balance between POP and PVGRF.

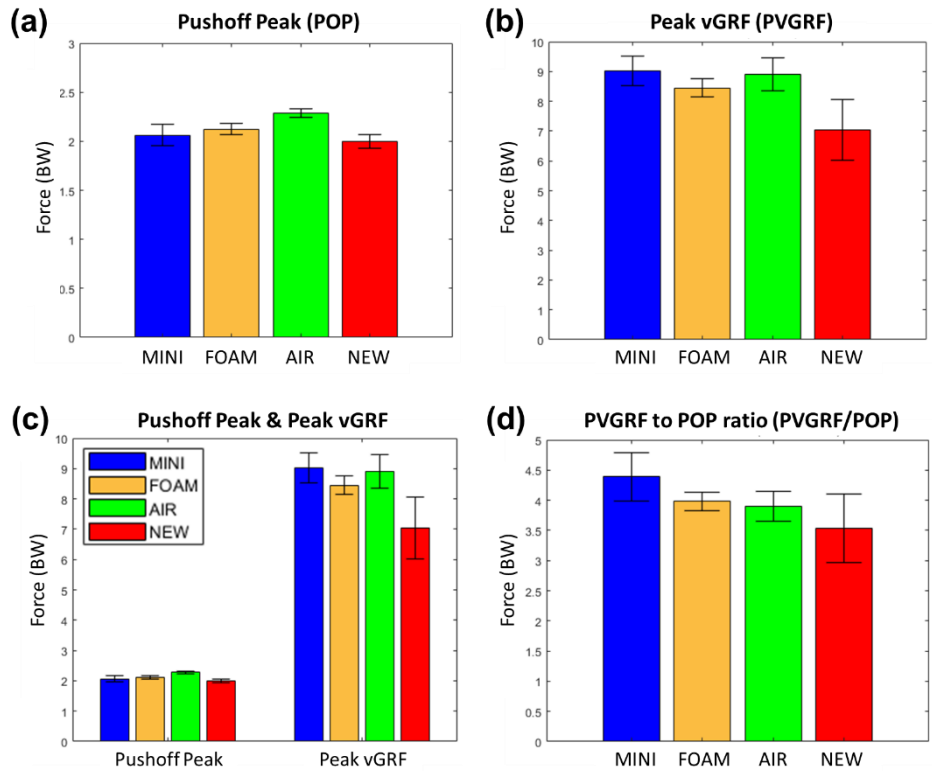

Figure 25. (a) Pushoff peak (POP), (b) peak vGRF (PVGRF),
(c) comparison of POP and PVGRF, and
(d) PVGRF to POP ratio (PVGRF/POP) of all footwear conditions.

The POP, or the maximum thrust force, of the proposed device was the lowest of all conditions, which was 3.1%, 5.8%, and 12% lower than that of MINI, FOAM, and AIR, respectively (Figure 25. (a)). Nevertheless, the increase in the shock absorption capability of the proposed device exceeds the decrease in the exercise efficiency. The proposed device exhibited the lowest PVGRF of all conditions, which was 22%, 17%, and 21% lower than that of MINI, FOAM, and AIR, respectively (Figure 25. (b)). The shoes except the proposed device herein denoted similar PVGRF values, and this result is comparable to the previous literature [10–12].

Moreover, the PVGRF to POP ratio (PVGRF/POP) was computed to analyze the landing impact at the same thrust force. The proposed device also demonstrated the best performance among all conditions

in this variable (Figure 25. (d)). Its PVGRF/POP was 20%, 11%, and 9.4% lower than that of MINI, FOAM, and AIR, respectively.

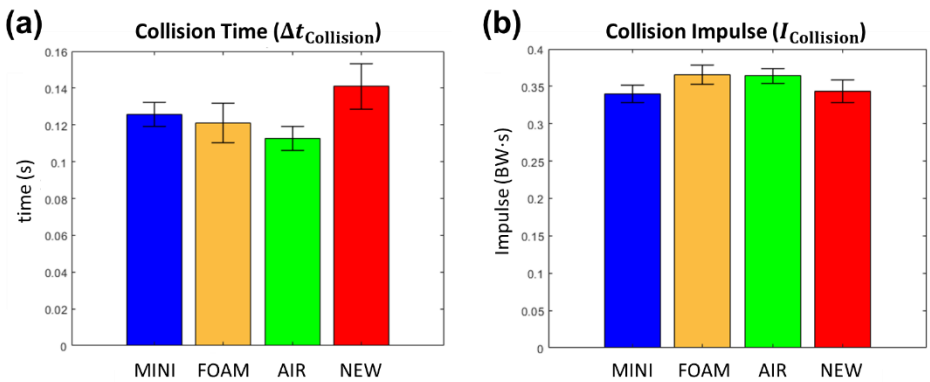

Figure 26. (a) Phase length and (b) impulse of the collision phase of all footwear conditions.

As the impulse of the collision phase, $I_{Collision}$, remains constant, the decrease in the VILR and the PVGRF of the proposed device suggests an increase in the collision time ($\Delta t_{Collision}$) (Equation (1)). The collision time of the proposed device was 12%, 17%, and 25% longer than that of MINI, FOAM, and AIR, respectively (Figure 26. (a)). On the other hand, its collision impulse ($I_{Collision}$) was 1.1% larger than that of MINI, but 6% smaller than those of FOAM and AIR (Figure 26. (b)). While the difference in the collision impulse between the footwear conditions was relatively small, the proposed device embodied the longest collision time of all conditions.

In summary, the proposed device presents the best shock absorption capability among all footwear conditions. This is caused by the change in the vGRF profile, which the PVGRF decreases and the collision time increases. (Hypothesis II)

3.3. Landing Stability

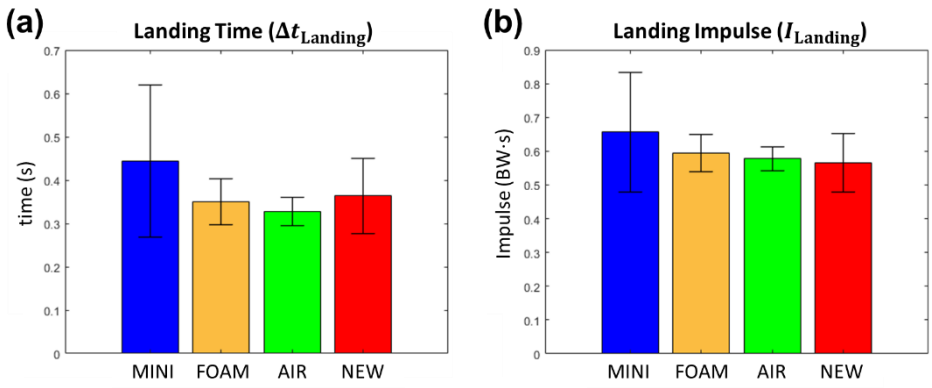

Figure 27. (a) Duration and (b) impulse of the landing process of all footwear conditions.

The landing time, $\Delta t_{\text{Landing}}$, represents the time required to stabilize the posture after the touchdown. Consequently, a shoe with short landing time has high landing stability. The landing time ($\Delta t_{\text{Landing}}$) of the proposed device was 18% shorter than that of MINI, while 4% and 11% longer than that of FOAM and AIR, respectively (Figure 27. (a)). In the meantime, its landing impulse (I_{Landing}) was the smallest of all conditions, which was 14%, 4.9%, 2.1% smaller than that of MINI, FOAM, and AIR, respectively (Figure 27. (b)). Namely, the proposed device disturbed the landing stability more than the cushioned shoes, but less than the minimalist shoes. Furthermore, it reduced the landing impulse by altering the vGRF profile.

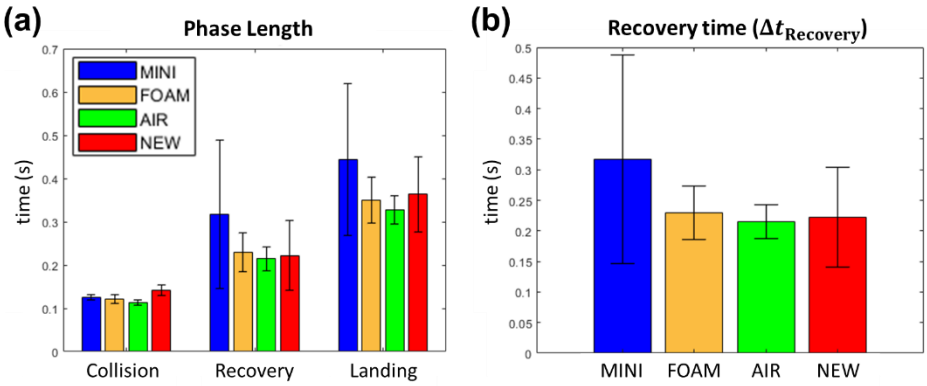

Figure 28. (a) Comparison of collision time, recovery time, and landing time of all footwear conditions.
(b) Duration of the recovery phase of all footwear conditions.

Although the proposed device exhibited the longest collision time of all conditions, its landing time did not increase as much as the collision time. This is caused by the change in the recovery time ($\Delta t_{\mathrm{Recovery}}$) (Figure 28. (b)). The recovery time of the proposed device was 3.6% longer than that of AIR, but 30% and 3.1% shorter than that of MINI and FOAM, respectively. Thus, its recovery time was akin to that of the cushioned shoes, but less than that of the minimalist shoes.

In short, the landing stability of the proposed device was little less than that of the common cushioned shoes, but substantially higher than that of the minimalist shoes. Hence, the proposed device moderately interferes with the stability while significantly absorbing shock during landing, compared to the other footwear conditions.

3.4. Kinematic Analysis

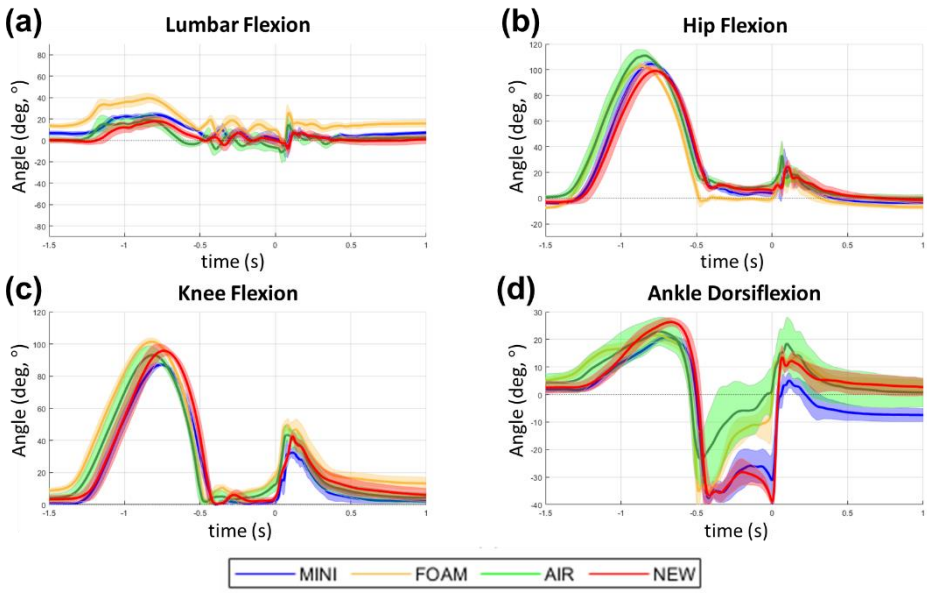

Figure 29. The joint angle profiles of all footwear conditions during the vertical countermovement jump: (a) lumbar flexion, (b) hip flexion, (c) knee flexion, and (d) ankle dorsiflexion. The solid blue, orange, green, and red lines represent the mean joint angle of MINI, FOAM, AIR, and NEW, respectively.

The lumbar flexion, hip flexion, and knee flexion angle profiles remained almost constant irrespective of the footwear conditions, but the ankle dorsiflexion angle profile did not (Figure 29.). It was obvious that the lumbar flexion did not fluctuate substantially, since the subject was instructed to straighten one's back during the CJ tasks. For the other joint angles, peaks and troughs near the key moments were contrasted to reveal the kinematic effect of the footwear conditions. The key moments are pushoff peak (POP), takeoff (TO), middle of the flight phase (FL), touchdown (TD), and active peak (AP).

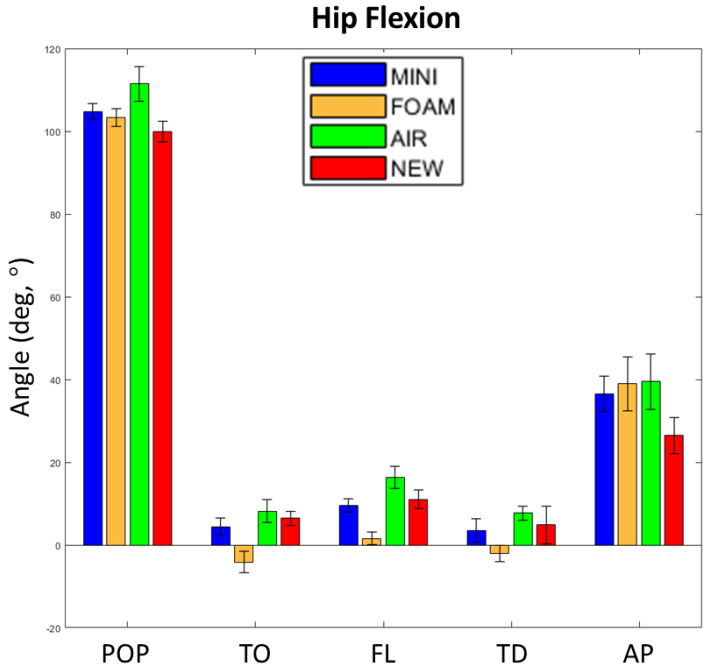

Figure 30. Comparison of the hip flexion angle profile of all footwear conditions.

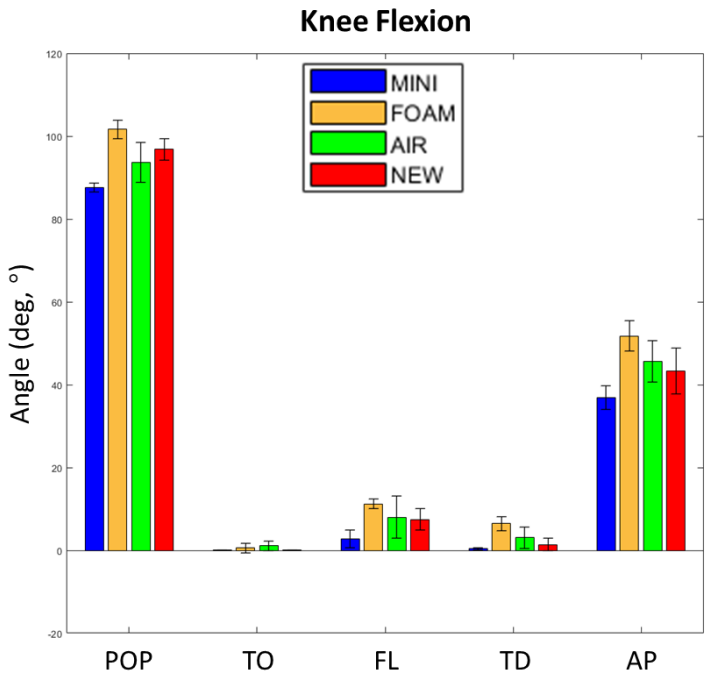

Figure 31. Comparison of the knee flexion angle profile of all footwear conditions.

The hip, knee, ankle muscles alleviate the landing impact via flexion moment. Specifically, the ankle muscles take a leading role in shock absorption during the stiff landing [33]. The proposed device showed the smallest hip flexion during landing, which was 35%, 47%, 32% smaller than that of MINI, FOAM, and AIR, respectively (Figure 30.). On the other hand, its knee flexion was 14% larger than that of MINI, while 7.5% and 1.6% smaller than that of FOAM and AIR, respectively (Figure 31.). Accordingly, the proposed device provokes the smallest flexion moment as far as the hip and knee joints are concerned.

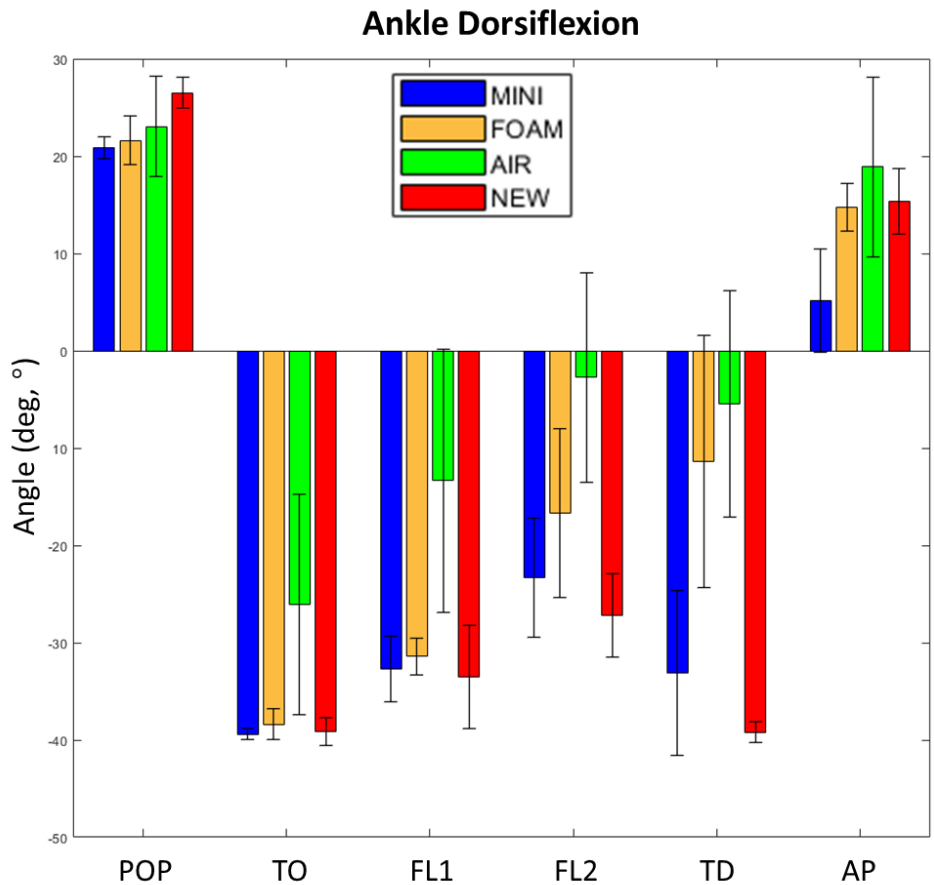

Figure 32. Comparison of the ankle dorsiflexion angle profile of all footwear conditions.

However, the proposed device aroused the largest flexion moment in the ankle joint (Figure 32.). Its ankle dorsiflexion during landing was 42%, 109%, and 124% larger than that of MINI, FOAM, and AIR, respectively. The increase in the ankle flexion moment of the proposed device outstrips the decrease in the hip and knee flexion moment, resulting in the best shock absorption performance among all footwear conditions.

Chapter 4. Discussion

This paper develops the pneumatic, variables stiffness cushioning system that attunes the mechanical properties in line with the jump landing phases. The proposed device is founded on two main hypotheses: change in the shoe hardness during landing can modify (1) the vGRF profile and (2) the collision time (Figure 2.). The overall results substantiate the hypotheses (Figure 22., 26.), and also indicate that the proposed device abates the VILR and the PVGRF (Figure 24., 25.). The propulsion assistance capability of the proposed device is lightly lower than that of the other footwear conditions. However, the increment in the shock absorption capacity substantially outweighs the decrement in the exercise efficiency (Figure 25.). The proposed device achieves the best shock absorption capacity by inducing the largest ankle flexion moment among all footwear conditions (Figure 32.). Moreover, the landing stability of the proposed device is akin to that of the other conditions (Figure 27.).

There are various opinions about the influence of the cushioning on the VILR. Some studies claim that the cushioning increases the VILR [11] and the others argues the opposite [39, 40]. However, the most studies, with a few exceptions [39], assert that the PVGRF does not change by the cushioning [10–12, 40]. In general, the cushioned shoes are deemed to have a limited effect on the landing impact. Nonetheless, the experimental results corroborate that the proposed device re-profiles the vGRF profile and considerably attenuates the landing impact.

It should be noted that the findings of this study are based on the results from the preliminary experiment. In addition, this study has concentrated on the jump landing, a basic element of the terrestrial locomotion. Besides, the tethered actuation system is required to activate the proposed device. Notwithstanding its limitations, this study introduces an innovative approach to the shock absorption during landing. To overcome the limitations of the existing

technologies, this study has concentrated on the vGRF profile during landing, not the specific parameters like the VILR and the PVGRF. In consequence, the proposed device creates a distinct change in the vGRF profile and successfully ameliorates the landing impact with reasonable stability. Further studies can complement the findings of this study by revamping the proposed device into an independent wearable system and conducting experiments on additional subjects and various sport activities.

Chapter 5. Conclusion

This paper proposes the shock-absorbing foot orthotic device using pneumatic variable stiffness actuators. The proposed device controls the spring and damping coefficients of the shoe cushions in accordance with the jump landing phases. The sensors built into the insoles detects the phases and the tethered actuation system regulates the shoe hardness by adjusting the cushion airflow. The horseshoe bellows cushions are made through the layered manufacturing process with the TPU-coated fabrics and the nonstick films. The experimental results demonstrate that the proposed device re-profiles the vGRF profile during landing and attenuates the landing impact with modest influence on the landing stability. This results in the marginally low propulsion assistance capacity of the proposed device compared to the commercial shoes. Nevertheless, a reduction in the collision force significantly outstrips that in the thrust force. This is accomplished by increase in the collision time and the ankle flexion moment. Future work will involve reorganizing the proposed device into an untethered wearable system, testing with additional subjects, and validating its efficacy on strenuous sport activities.

Bibliography

[1] T. S. Keller, A. M. Weisberger, J. L. Ray, S. S. Hasan, R. G. Shiavi, and D. M. Spengler, "Relationship between vertical ground reaction force and speed during walking, slow jogging, and running," *Clinical Biomechanics*, vol. 11, no. 5, pp. 253–259, 1996.

[2] H. M. Ericksen, P. A. Gribble, K. R. Pfile, and B. G. Pietrosimone, "Different modes of feedback and peak vertical ground reaction force during jump landing: a systematic review," *Journal of Athletic Training*, vol. 48, no. 5, pp. 685–695, 2013.

[3] J. S. Dufek and B. T. Bates, "Biomechanical factors associated with injury during landing in jump sports," *Sports Medicine*, vol. 12, no. 5, pp. 326–337, 1991.

[4] J. Gray, J. E. Taunton, D. C. McKenzie, D. B. Clement, J. P. McConkey, and R. G. Davidson, "A survey of injuries to the anterior cruciate ligament of the knee in female basketball players," *International Journal of Sports Medicine*, vol. 6, no. 6, pp. 314–316, 1985.

[5] T. E. Hewett, G. D. Myer, K. R. Ford, R. S. Heidt Jr, A. J. Colosimo, S. G. McLean, A. J. van den Bogert, M. V. Paterno, and P. Succop, "Biomechanical measures of neuromuscular control and valgus loading of the knee predict anterior cruciate ligament injury risk in female athletes: a prospective study," *The American Journal of Sports Medicine*, vol. 33, no. 4, pp. 492–501, 2005.

[6] A. A. Zadpoor and A. A. Nikooyan, "The relationship between lower–extremity stress fractures and the ground reaction force: a systematic review," *Clinical Biomechanics*, vol. 26, no. 1, pp. 23–28, 2011.

[7] H. van der Worp, J. W. Vrielink, and S. W. Bredeweg, "Do runners who suffer injuries have higher vertical ground reaction forces than those who remain injury–free? A systematic review and meta–analysis," *British Journal of Sports Medicine*, vol. 50, no. 8, pp. 450–457, 2016.

[8] A. J. Fox, F. Wanivenhaus, A. J. Burge, R. F. Warren, and S. A. Rodeo, "The human meniscus: a review of anatomy, function, injury, and advances in treatment," *Clinical Anatomy*, vol. 28, no. 2, pp. 269–287, 2015.

[9] M. A. Lafortune, E. M. Hennig, and M. J. Lake, "Dominant role of interface over knee angle for cushioning impact loading and regulating initial leg stiffness," *Journal of Biomechanics*, vol. 29, no. 12, 1523–1529, 1996.

[10] D. E. Lieberman, M. Venkadesan, W. A. Werbel, A. I. Daoud, S. D 'andrea, I. S. Davis, R. O. Mang'Eni, and Y. Pitsiladis, "Foot strike patterns and collision forces in habitually barefoot versus shod runners," *Nature*, vol. 463, no. 7280, pp. 531–535, Jan, 2010.

[11] J. P. Kulmala, J. Kosonen, J. Nurminen, and J. Avela, "Running in highly cushioned shoes increases leg stiffness and amplifies impact loading," *Scientific Reports*, vol. 8, no. 1, pp. 1–7, Nov, 2018.

[12] J. W. LaPorta, L. E. Brown, J. W. Coburn, A. J. Galpin, J. J. Tufano, V. L. Cazas, and J. G. Tan, "Effects of different footwear on vertical jump and landing parameters," *The Journal of Strength and Conditioning Research*, vol. 27, no. 3, pp. 733–737, 2013.

[13] B. Nigg, M. Mohr, and S. R. Nigg, "Muscle tuning and preferred movement path–a paradigm shift," *Current Issues in Sport Science (CISS)*, 2017.

[14] D. P. Ferris, M. Louie, and C. T. Farley, "Running in the real world: adjusting leg stiffness for different surfaces," *Proceedings of the Royal Society of London. Series B: Biological Sciences*, vol. 265, no. 1400, pp. 989–994, 1998.

[15] D. P. Ferris and C. T. Farley, "Interaction of leg stiffness and surface stiffness during human hopping," *Journal of Applied Physiology*, vol. 82, no. 1, pp. 15–22, 1997.

[16] S. J. Crenshaw, F. E. Pollo, and E. F. Calton, "Effects of lateral–wedged insoles on kinetics at the knee," *Clinical Orthopaedics and Related Research*, vol. 375, pp. 185–192,

2000.

[17] W. Kakihana, M. Akai, K. Nakazawa, T. Takashima, K. Naito, and S. Torii, "Effects of laterally wedged insoles on knee and subtalar joint moments," *Archives of Physical Medicine and Rehabilitation*, vol. 86, no. 7, pp. 1465–1471, 2005.

[18] D. S. Fisher, C. O. Dyrby, A. Mündermann, E. Morag, and T. P. Andriacchi, "In healthy subjects without knee osteoarthritis, the peak knee adduction moment influences the acute effect of shoe interventions designed to reduce medial compartment knee load," *Journal of Orthopaedic Research*, vol. 25, no. 4, pp. 540–546, 2007.

[19] J. C. Erhart, A. Mündermann, B. Elspas, N. J. Giori, and T. P. Andriacchi, "A variable–stiffness shoe lowers the knee adduction moment in subjects with symptoms of medial compartment knee osteoarthritis," *Journal of Biomechanics*, vol. 41, no. 12, pp. 2720–2725, 2008.

[20] K. A. Boyer, P. Federolf, C. Lin, B. M. Nigg, and T. P. Andriacchi, "Kinematic adaptations to a variable stiffness shoe: Mechanisms for reducing joint loading," *Journal of Biomechanics*, vol. 45, no. 9, pp. 1619–1624, 2012.

[21] J. C. Erhart-Hledik, G. B. Mahtani, J. L., Asay, E. Migliore, M. M. Nguyen, T. P. Andriacchi, and C. R. Chu, "Changes in knee adduction moment wearing a variable-stiffness shoe correlate with changes in pain and mechanically stimulated cartilage oligomeric matrix levels," *Journal of Orthopaedic Research*, vol. 39, no. 3, pp. 619–627, 2021.

[22] M. K. Shepherd and E. J. Rouse, "The VSPA foot: A quasi–passive ankle–foot prosthesis with continuously variable stiffness," *IEEE Transactions on Neural Systems and Rehabilitation Engineering*, vol. 25, no. 12, pp. 2375–2386, 2017.

[23] C. Lecomte, A. L. Ármannsdóttir, F. Starker, H. Tryggvason, K. Briem, and S. Brynjolfsson, "Variable stiffness foot design and validation," *Journal of Biomechanics*, vol. 122, pp. 110440, 2021.

[24] S. O. Schrade, K. Dätwyler, M. Stücheli, K. Studer, D. A. Türk, M. Meboldt, R. Gassert, and O. Lambercy, "Development of VariLeg, an exoskeleton with variable stiffness actuation: first results and user evaluation from the CYBATHLON 2016," *Journal of Neuroengineering and Rehabilitation*, vol. 15, no. 1, pp. 1–18, 2018.

[25] A. A. Nikooyan and A. A. Zadpoor, "Mass–spring–damper modelling of the human body to study running and hopping–an overview," *Proceedings of the Institution of Mechanical Engineers, Part H: Journal of Engineering in Medicine*, vol. 225, no. 12, pp. 1121–1135, 2011.

[26] W. Liu and B. M. Nigg, "A mechanical model to determine the influence of masses and mass distribution on the impact force during running," *Journal of Biomechanics*, vol. 33, no. 2, pp. 219–224, 2000.

[27] A. A. Zadpoor and A. A. Nikooyan, "Modeling muscle activity to study the effects of footwear on the impact forces and vibrations of the human body during running," *Journal of Biomechanics*, vol. 43, no. 2, pp. 186–193, 2010.

[28] A. A. Nikooyan and A. A. Zadpoor, "An improved cost function for modeling of muscle activity during running," *Journal of Biomechanics*, vol. 44, no. 5, pp. 984–987, 2011.

[29] K. E. Zelik and A. D. Kuo, "Mechanical work as an indirect measure of subjective costs influencing human movement," *PLoS ONE*, vol. 7, no. 2, 2012.

[30] W. Niu, M. Zhang, Y. Fan, and Q. Zhao, "Dynamic postural stability for double–leg drop landing," *Journal of Sports Sciences*, vol. 31, no. 10, pp. 1074–1081, 2013.

[31] W. Niu, Y. Wang, Y. He, Y. Fan, and Q. Zhao, "Kinematics, kinetics, and electromyogram of ankle during drop landing: a comparison between dominant and non–dominant limb," *Human Movement Science*, vol. 30, no. 3, pp. 614–623, 2011.

[32] H. D. Yang and A. T. Asbeck, "A Layered Manufacturing Approach for Soft and Soft–Rigid Hybrid Robots," *Soft Robotics*, vol. 7, no. 2, pp. 218–232, 2020.

[33] P. Devita and W. A. Skelly, "Effect of landing stiffness on joint kinetics and energetics in the lower extremity," *Medicine and Science in Sports and Exercise*, vol. 24, no. 1, pp. 108–115, 1992.

[34] M. Paulich, M. Schepers, N. Rudigkeit, and G. Bellusci, "Xsens MTw Awinda: Miniature wireless inertial–magnetic motion tracker for highly accurate 3D kinematic applications," *Xsens: Enschede, The Netherlands*, pp. 1–9, 2018.

[35] G. Street, S. McMillan, W. Board, M. Rasmussen, and J. M. Heneghan, "Sources of error in determining counter–movement jump height with the impulse method," *Journal of Applied Biomechanics*, vol. 17, no. 1, pp. 43–54, 2001.

[36] S. L. Delp, F. C. Anderson, A. S. Arnold, P. Loan, A. Habib, C. T. John, E. Guendelman, and D. G. Thelen, "OpenSim: open–source software to create and analyze dynamic simulations of movement," *IEEE Transactions on Biomedical Engineering*, vol. 54, no. 11, pp. 1940–1950, 2007.

[37] A. Rajagopal, C. L. Dembia, M. S. DeMers, D. D. Delp, J. L. Hicks, and S. L. Delp, "Full–body musculoskeletal model for muscle–driven simulation of human gait," *IEEE Transactions on Biomedical Engineering*, vol. 63, no. 10, pp. 2068–2079, 2016.

[38] T. Ueda, H. Hobara, Y. Kobayashi, T. A. Heldoorn, M. Mochimaru, and H. Mizoguchi, "Comparison of 3 methods for computing loading rate during running," *International Journal of Sports Medicine*, vol. 37, no. 13, pp. 1087–1090, 2016.

[39] L. Malisoux, P. Gette, A. Urhausen, J. Bomfim, and D. Theisen, "Influence of sports flooring and shoes on impact forces and performance during jump tasks," *PLoS ONE*, vol. 12, no. 10, 2017.

[40] J. J. Hannigan and C. D. Pollard, "Comparing walking biomechanics of older females in maximal, minimal, and traditional shoes, " *Gait & Posture*, vol. 83, pp. 245–249, 2021.

Abstract in Korean

공압 가변 강성 액추에이터를 이용한 충격을 흡수하는 발 지지 장치

박 영 준

서울대학교 기계공학부 대학원

육상 이동은 일상생활동작 (ADL; activities of daily living) 에 있어서 필수불가결한 요소이다. 그리고 이는 추진, 비행, 착지의 일련의 위상들로 이루어진다. 이동 도중 지면반력 (GRF; ground reaction force) 은 추진력으로써 인간의 운동 성능을 향상시키지만, 동시에 충돌력으로써 안전을 저해하는 이중성을 갖고 있다. 쿠션 신발은 과도한 수직 지면반력 (vGRF; vertical ground reaction force) 으로 인한 하지 부상을 방지할 수 있다고 여겨져 왔다. 그러나 최근 연구들은 신발 강성이 최대 수직 지면반력 (PVGRF; peak vGRF) 을 변화시키지 못한다고 주장하며, 이러한 통념을 반박하고 있다. 이러한 차이는 신발을 포함한 하반신 전체 강성이 항상 일정하며 쿠션의 용수철과 같은 특성이 그 충격 흡수 능력을 상쇄시킨다는 “근육 조율” 패러다임으로 설명된다. 본 논문은 착지 도중 수직 지면반력 개형을 재구성할 수 있는 혁신적인 충격 흡수 발 지지 장치를 제안한다. 제안된 장치는 다음 두가지 핵심 가설들에 토대를 두고 있다: 착지 도중 신발 강성의 변화는 (1) 수직 지면반력 개형과 (2) 충돌 시간을 변화시킬 수 있다. 발 맞춤형, 말발굽 풀무 모양 쿠션들은 적층식 제조 공정을 통해 제작되었으며, 시판 미니멀리스트 신발 바닥에 부착되었다. 본 장치는 신발 안창 아래에 내장된 센서들을 통해 점프 착지 동작의 위상들을 식별하고, 해당 위상들에 따라 쿠션의 스프링 및 감쇠 계수들을 조절한다. 기계적 특성 변화는 쿠션의 공기 흐름 제어를 통해 구현된다. 본 논문은 제안된 장치의 유효성을 평가하고, 이를 다음 세가지 시판

신발들과 비교하기 위해 한 명의 연구참여자에 대하여 예비 실험을 수행하였다: 미니멀리스트 신발 (MINI), 폼 쿠션 신발 (FOAM), 그리고 공기 쿠션 신발 (AIR). 종합 실험 결과는 앞서 세운 가설들을 확증하였으며, 제안된 장치가 모든 신발들 중에서 가장 좋은 충격 흡수 능력을 가졌음을 시사하였다. 본 장치는 가장 낮은 수직 순간 하중 증가율 (VILR; vertical instantaneous loading rate) 을 나타내었으며, 이는 MINI, FOAM, AIR 보다 각각 62%, 34%, 24% 낮았다. 마찬가지로, 본 장치의 최대 수직 지면반력 (PVGRF) 은 MINI, FOAM, AIR 보다 각각 22%, 17%, 21% 낮아, 모든 신발들 중 가장 낮았다. 이로 인해 추진 보조가 약간 감소하였으나, 충돌력의 감소량이 추진력의 감소량을 크게 상회하였다. 본 장치의 최대 추진력 (POP; pushoff peak) 은 MINI, FOAM, AIR 보다 각각 3.1%, 5.8%, 12% 낮아 최소치를 기록하였다. 그러나 본 장치는 모든 신발들 중 가장 낮은 최대 추진력 대비 최대 수직 지면반력의 비율 (PVGRF/POP), 다시 말해 동일 추진력 대비 가장 낮은 착지 충격을 나타내었으며, 이는 MINI, FOAM, AIR 보다 각각 3.1%, 5.8%, 12% 낮았다. 이러한 결과는 충돌 시간과 발목 굽힘 모멘트의 증가에서 기인하였다. 본 장치의 충돌 시간은 모든 신발들 중 가장 길었으며, 이는 MINI, FOAM, AIR 보다 각각 12%, 17%, 25% 길었다. 또한, 본 장치는 착지 도중 가장 큰 발목 발등 굽힘을 유발하였으며, 이는 MINI, FOAM, AIR 보다 각각 42%, 109%, 124% 큰 값이었다. 그럼에도 불구하고, 착지 안정성에 본 장치가 미친 영향은 다른 신발들과 유사하였다. 본 장치의 착지 시간은 MINI 보다 18% 짧았으나, FOAM 과 AIR 보다 각각 4%, 11% 길었다. 한편, 본 장치의 착지 충격량은 모든 신발들 중 가장 작았으며, 이는 MINI, FOAM, AIR 보다 각각 14%, 4.9%, 2.1% 작았다. 향후 연구에서는 제안된 장치를 독립된 무선 웨어러블 시스템으로 재구성하고, 추가 연구참여자들에게 실험을 수행하며, 격렬한 스포츠 도중 본 장치의 효과를 입증할 것이다.

주요어 : 충격 흡수, 발 지지 장치, 수직 지면반력 개형,
쿠션, 가변 강성, 공압 구동기

학번 : 2019-22678